animals were placed in a temperature-controlled chamber until thermoregulation was reestablished. Manual bladder expression was performed twice per day until reflex bladder emptying was reestablished.

Injection of MR16-1 and BrdU

Immediately after the SCI, mice were intraperitoneally injected with a single dose of MR 16-1 (100 μg/g body weight; MR16-1 group) or with the same volume and concentration of purified rat IgG (ICN/Cappel Ohio; control group). To label the cells that divided after the injury, a sterile solution of bromodeoxyuridine (BrdU; 50 μg/g body weight; Sigma) was intraperitoneally injected daily for 2 weeks after the SCI.

Behavioral Analysis

Three different tests were used to assess recovery of motor function after SCI. We examined 30 injured mice (15 animals per group) for functional evaluation. Each mouse was tested at 1, 3, 5, and 7 days postoperatively and weekly thereafter until 6 weeks. Every test was performed in a double-blind fashion and recorded on videotape.

Open-field locomotion. Motor function of the hindlimbs was evaluated by the locomotor rating test on the Basso-Beattie-Bresnahan (BBB) scale, as described previously (Basso et al., 1996). A team of three experienced examiners evaluated each animal for 4 min and assigned an operationally defined score for each hindlimb.

SCANET. Motor function was evaluated with a SCANET automated motion-analysis system (MV-10, Toyo Sangyo Co., Ltd., Toyama, Japan) developed to measure spontaneous motor activity in small animals. SCANET consists of a cage equipped with two crossing sensor frames arranged at different heights that allow monitoring of small (M1) and large (M2) horizontal movements plus the vertical movement involved in rearing (RG). The M1 and M2 scores represent total distances moved, and the RG score represents the frequency of vertical movements within a certain period, which is useful for assessing recovery of limb function after SCI in mice, as reported previously (Mikami et al., 2002). Each mouse was individually placed in the SCANET cage, and its spontaneous locomotor activity was measured for 10 min.

Rota-rod treadmill. Motor coordination was assessed with a rotating rod apparatus (Muromachi Kikai Co., Ltd., Tokyo, Japan), consisting of a plastic rod (3 cm diameter, 8 cm long) with a gritted surface, flanked by two large discs (40 cm diameter). A mouse was placed on the rod, and the rod was rotated at speeds of 5, 10, and 15 rpm. Latency until a fall occurred was monitored for 120 sec (Ogura et al., 2001). Three trials were conducted at each speed, and the average and maximum numbers of seconds were recorded.

Immunohistochemistry

At 2 weeks after the SCI, animals in both the MR16-1 group and the control group were deeply anesthetized by inhalation of diethyl ether and transcardially perfused with 4% paraformaldehyde in 0.1 M phosphate-buffered saline (PBS) for histological studies. Spinal cord tissue was removed and post-fixed with 4% paraformaldehyde in PBS for a few hours at room temperature. Tissue samples were immersed in 10% sucrose in PBS at 4°C for 24 hr, placed in 30% sucrose in PBS for 48 hr, and embedded in OTC compound. The embedded tissue was immediately frozen in liquid nitrogen and stored at −80°C until needed. Frozen sections of spinal cord 20 μm thick were cut on a cryostat in the axial and sagittal plane and stained with hematoxylin and eosin. For the immunofluorescence double-labeling experiment, spinal cord sections were permeabilized with 0.03% Triton X-100 and 10% normal goat serum in 0.01 M PBS, pH 7.4, for 30 min. As primary antibodies, rat anti-BrdU 1:200 (Abcam, Cambridge, United Kingdom), rabbit anti-GFAP antibody 1:1000 (Dako, Carpinteria, CA), rat anti-Mac-1 1:200 (Pharmingen, San Diego, CA), or human anti-Hu 1:2,000 (a gift from Dr. Robert Darnell, The Rockefeller University) were applied to the sections at 4°C overnight. The sections were then incubated with secondary antibodies conjugated with Texas red, fluorescein isothiocyanate (FITC; all from Jackson Immunoresearch, West Grove, PA) for 1 hr at room temperature. The slides were then washed, wet mounted, and examined under a fluorescence microscope. For diaminobenzidine (DAB; Sigma) staining, rat anti-Mac-1 antibody 1:200 (Pharmingen) was used as the primary antibody, followed by a horseradish peroxidase (HRP)-labeled goat anti-rat IgG as the secondary antibody. Staining was visualized with DAB, and slides were washed, dehydrated, cleared in xylene, and mounted. For the in vitro study, cells cultured on chamber slides were fixed with 4% paraformaldehyde in PBS and subjected to immunofluorescence staining. Rabbit anti-GFAP antibody 1:1,000 (Dako) was used as the primary antibody, followed by FITC-conjugated goat anti-rabbit IgG as the secondary antibody. The cells were counterstained with Hoechst 33258 to identify nuclei.

Quantitative Analysis

Images were obtained by fluorescence microscopy (Axioskop 2 plus; Carl Zeiss Co., Ltd., Tokyo, Japan). For quantification of connective tissue scar (CTS) formation in vivo, five representative axial sections, 1.0 mm and 0.5 mm rostral to the lesion epicenter, at the lesion epicenter, and 0.5 mm and 1.0 mm caudal to the lesion epicenter were selected from a 4-mm length of cord, centered over the impact site, and the CTS area was measured using NIH Image software in H&E-stained sections and calculated as a percentage of the total axial area. To evaluate astrogliosis, five representative axial sections were selected as described above, and six regions in each section were captured randomly at ×200 magnification by confocal microscopy (LSM510; Carl Zeiss Co., Ltd.). The glial fibrillary acidic protein (GFAP)/BrdU double-positive cells in each region were counted by three investigators in a blinded fashion, and the density of each section (number of GFAP/BrdU double-positive cells per total axial area) was calculated. To quantify the proportion of the lesion that was Mac-1 immunolabeled, five representative midsagittal sections (3 mm long) were selected, and the immunoreactive area was measured with the MCID system (Imaging Research, Inc., Troonto, Ontario, Canada).

Western Blot Analysis

At 12 hr after the injury, spinal cord tissue of the lesion epicenter (6 mm long) was dissected from the mice (four animals per group and four sham-operated animals), homogenized in MAPK lysis buffer containing protease inhibitor, and after son-

ication centrifuged at 15,000 rpm. Protein from the supernatant of each sample was separated by 10% SDS-PAGE and transferred to polyvinylidene difluoride membranes by electrophoresis. The membranes were blocked for 1 hr at room temperature in TBST buffer containing 4% nonfat milk, NaCl (150 mM), and 0.05% Tween 20. The blots were then incubated with either primary polyclonal rabbit anti-stat3 antibody, rabbit antiphospho-stat3 antibody 1:500 (Cell Signaling Technology, Beverly, MA), mouse anti-α-tubulin antibody 1:500, or rabbit anti IL-6Rα antibody 1:200 (Santa Cruz Biotechonology, Santa Cruz, CA), followed by a secondary HRP-conjugated anti-rabbit or mouse IgG antibody. The blots were visualized with the ECL Blotting Analysis System (Amersham, Arlington Heights, IL).

Statistical Analysis

Values are reported as means ± SEM. Differences in all tests except for the rearing score analysis were analyzed for statistical significance by the unpaired Student's *t*-test. SCANET rearing scores were compared between groups by ANOVA with the post hoc Fisher's exact test. In all statistical analyses, significance was accepted at $P = .05$.

RESULTS

Effect of MR16-1 on Neural Stem/Progenitor Cells In Vitro

We investigated the effect of IL-6 signaling and MR16-1 on NSPC differentiation in vitro by performing the differentiation assay on adult spinal cord-derived neural precursor cells that had been expanded in a floating culture according to a previously reported method (Reynolds and Weiss, 1992; Shimazaki et al., 2001). Approximately 47.1% of the control NSPCs cultured in medium alone differentiated into astrocytes (Fig. 1A1,B). After addition of IL-6 and sIL-6R to induce gp130-mediated signaling (Taga et al., 1989; Tamura et al., 1993), NSPC differentiation into astrocytes was enhanced, and there was obvious extension of GFAP-positive processes (Fig. 1A2,B). By contrast, addition of MR16-1 to IL-6 plus sIL-6R inhibited the effect of IL-6 plus sIL-6R on astrocytic differentiation (Fig. 1A3), and there was a significant decrease in GFAP-positive cells as a percentage of total live cells in the MR16-1 group compared with the IL-6 plus sIL-6R-alone-treated group (mean value of 43.2% ± 2.8% in the MR16-1 group compared with 64.9% ± 3.5% in the IL-6 plus sIL-6R group; Fig. 1B). There was no significant difference in the number of total live cells between these two groups. These results indicate that the astrocytic differentiation-promoting effect of the IL-6 signal was sufficiently blocked by MR16-1 in vitro.

Histological Changes in Mice After SCI

Two weeks after the SCI, there was no cavitation at the lesion epicenter, but the central gray matter had been completely replaced by CTS in both the control group and the MR16-1 groups (Fig. 2). Single or double immunostaining was then performed to determine composition of the cells at the lesion site. Mac-1-positive inflammatory cells were observed mainly in the scar area (Fig. 2H,I), and Hu-positive neurons were found to remain only in the spared white matter (Fig. 2E,F) compared with uninjured mice (Fig. 2D,G). On the other hand, there were few GFAP-positive cells within the central lesion area, and it was surrounded by GFAP-positive astrocytes in both the axial and the sagittal sections (Fig. 3). We found that the area of the CTS was essentially GFAP negative. Interestingly, the CTS area was smaller in the MR16-1 group (Fig. 3B,D) than in the control group (Fig. 3A,C). Double immunostaining with GFAP and BrdU revealed BrdU in the nuclei of the GFAP-positive cells, indicating that they had divided after the SCI, and they were concluded to be reactive astrocytes.

To determine whether administration of MR16-1 suppressed astrogliosis after SCI, we counted the numbers of GFAP and BrdU double-positive cells at the epicenter and 0.5 and 1.0 mm rostral and caudal to the epicenter (Fig. 4). Representative confocal images of the lesioned area under higher magnification are shown in Figure 4A (control group) and 4B (MR16-1 group). In the MR16-1 group, there were significantly fewer GFAP and BrdU double-positive cells than in the control group (mean of 85.1 ± 2.5 cells/mm^2 in the control group compared with 63.3 ± 9.3 cells/mm^2 in the MR16-1 group; Fig. 4C).

Western Blotting

We confirmed the significantly increased expression of the IL-6 receptor in the injured spinal cord by Western blot analysis. In the intact spinal cord of sham-operated mice (in which only laminectomy was performed), the expression level of the IL-6 receptor was very low. However, the expression level had increased by nearly eightfold at 12 hr after the injury (Fig. 5A,C). To investigate whether the decrease in reactive astrocytes was due to blockade of the IL-6 signal cascade, we performed an analysis of both the total and the phosphorylated forms of the signal transducer and activator of transcription 3 (STAT3), a principal part of the IL-6 family signal cascade. Initiation of IL-6 signaling occurs when IL-6 binds to the IL-6R, which leads to association with gp130, and this receptor complex leads to activation of gp130-associated tyrosine kinases (JAK kinases). JAK activation then leads to tyrosine phosphorylation of STATs (Taga and Kishimoto, 1997; Van Wagoner and Benveniste, 1999; Ohtani et al., 2000). Upon phosphorylation, STAT3 proteins dimerize and translocate to the nucleus, where they bind to elements in the promoter of GFAP genes (Bonni et al., 1997), so quantification of phosphorylated STAT3 is an adequate index of the extent of IL-6 signaling. Administration of MR16-1 decreased the expression of phosphorylated STAT3 compared with the control group (Fig. 5B), and there was a significant difference in the ratio of phosphorylated to total STAT3 expression between the control group and the MR16-1 group (Fig. 5D). These findings suggested that the intraperitoneally injected MR16-1 actually blocked the IL-6/JAK/STAT3 signaling pathway and suppressed astrogliosis after SCI. However, strictly speaking, the alternative possibility that the observed reduction in the phosphorylated STAT3 level in the MR16-

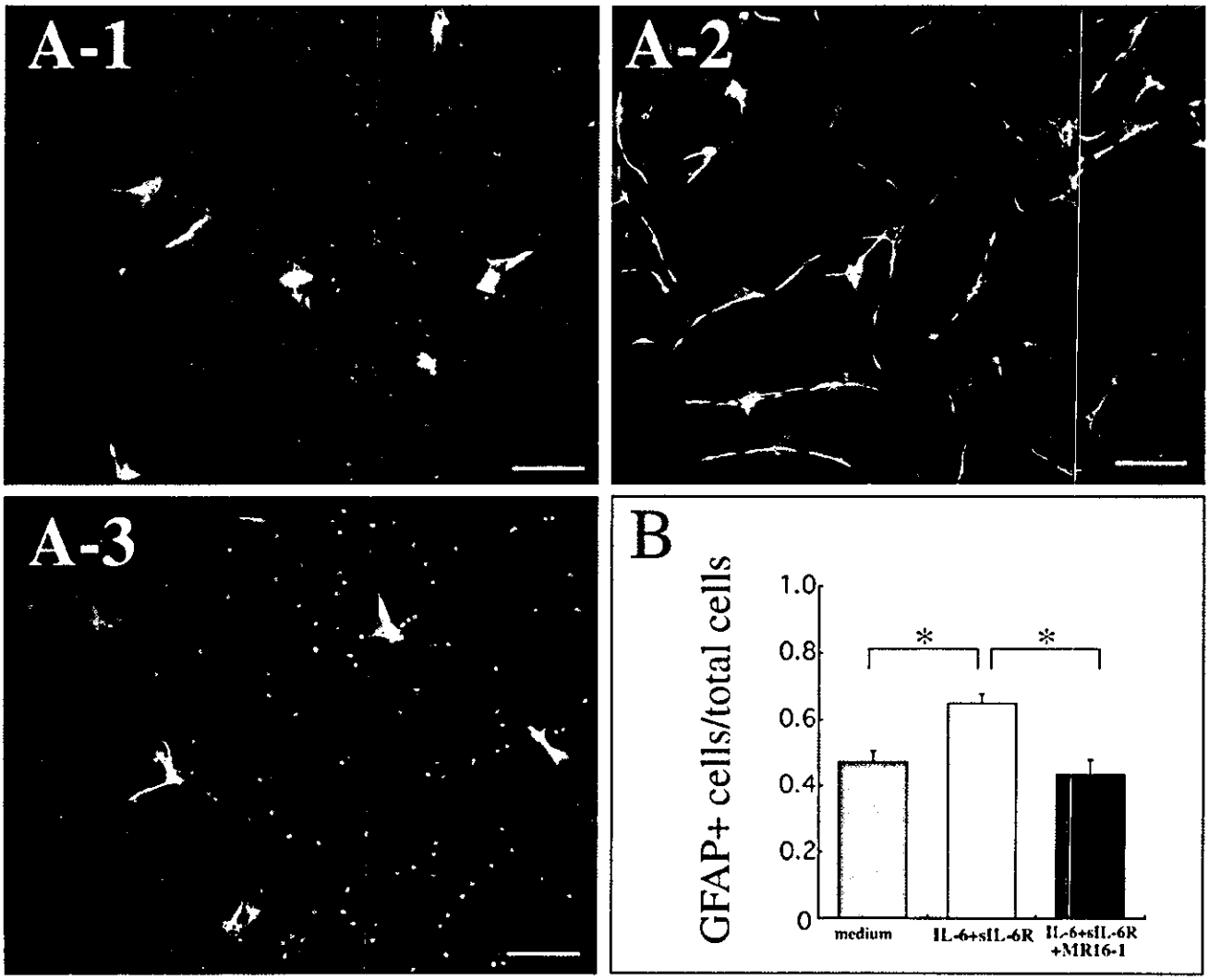

Fig. 1. Effect of the IL-6 signal and MR16-1 on the astrocytic differentiation of NSPCs. **A:** Dissociates of neural progenitor cells were cultured for 3 days with medium alone (A1), IL-6 and soluble IL-6 receptor at 20 ng/ml (A2), and IL-6 and soluble IL-6 receptor plus MR16-1 at 20 μg/ml (A3) and then subjected to immunofluorescence staining for GFAP (green) and Hoechst 33258 (blue). **B:** The number of GFAP-positive cells was calculated as a percentage of all live cells. Values are means ± SEM. $*P < .05$; two-tailed t-test ($n = 3$). Scale bars = 50 μm.

1-treated group resulted from suppression of astrogliosis by some unknown mechanisms cannot be excluded.

MR16-1 Suppressed the Infiltration by Inflammatory Cells After SCI

In addition to regulation of the astrocytic differentiation of NSPCs, IL-6 plays critical roles as a proinflammatory cytokine that activates macrophages and induces inflammatory cell chemotaxis and fibroblast proliferation (Romano et al., 1997; Van Wagoner and Benveniste, 1999; Tuna et al., 2001). To determine the antiinflammatory effect of MR16-1, we therefore performed immunolabeling of Mac-1-positive cells in sagittal sections at the lesion epicenter. Fewer Mac-1-positive cells were observed at the lesion epicenter 2 weeks after the injury in the MR16-1 group (Fig. 6A,B), and quantitative analysis showed statistically significant differences Mac-1-immunolabeled area in the MR-16 group and in the control group (mean of 5.6% ± 1.0% in the MR16-1 group, compared with 15.1% ± 1.2% in the control group; Fig. 6C). We also measured the area of the CTS after SCI using NIH Image software in H&E-stained serial sections and found that the area of the scar at the lesion epicenter 2 weeks after injury was significantly smaller in the MR16-1 mice (mean 47.4% ± 1.3% in the MR16-1 group compared with 64.5% ± 2.7% in the control group; Fig. 6D). These results indicate that administration of MR16-1 attenuated the inflammatory responses following injury in vivo.

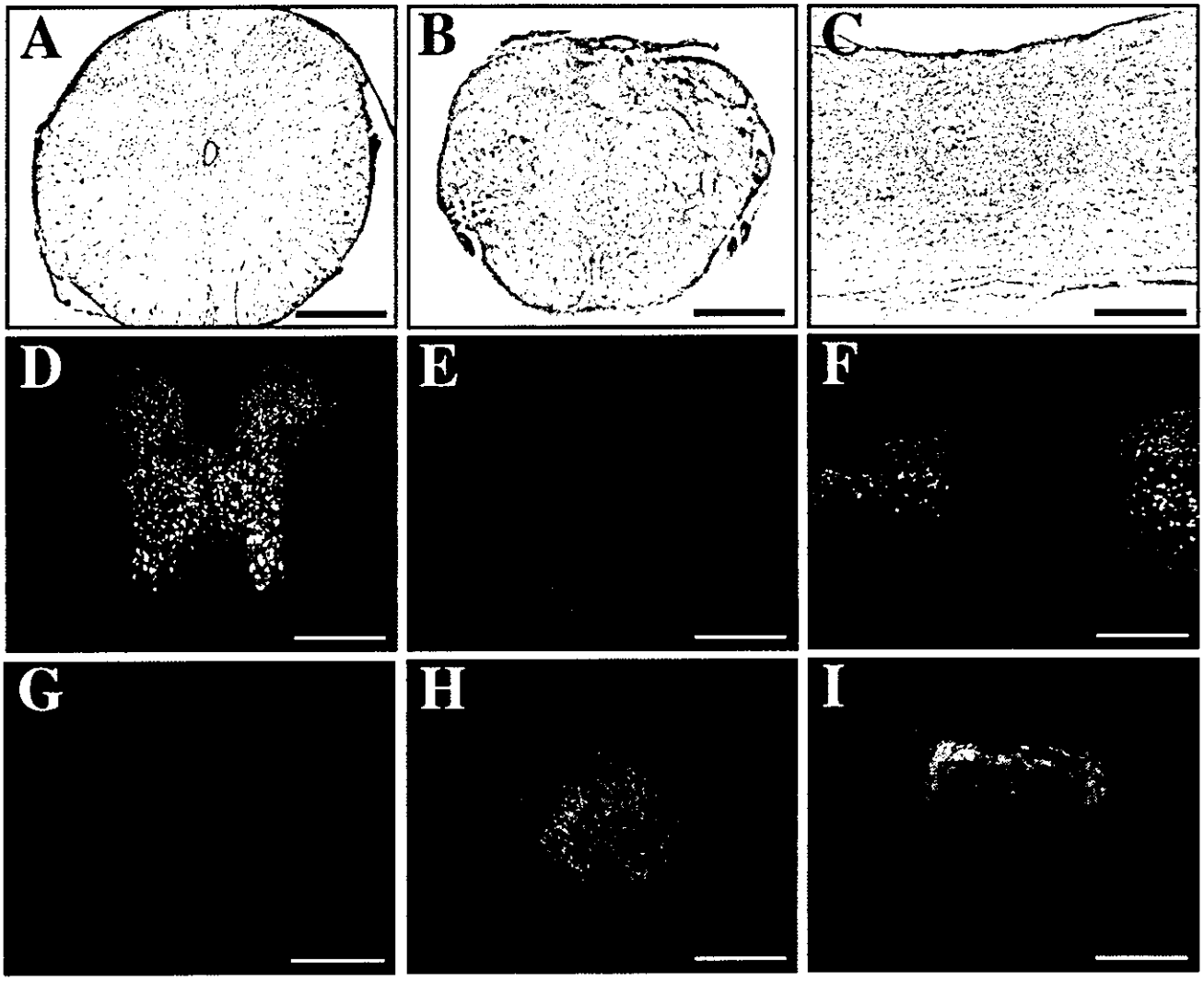

Fig. 2. Photomicrographs of representative immunohistochemistry and H&E-stained sections from the lesion epicenter 2 weeks after injury obtained from the MR16-1 group (B,C,E,F,H,I) and normal mice (A,D,G). **A–C:** H&E staining showed that the normal gray matter in the lesion epicenter had been completely replaced by a connective tissue scar. **D–F:** Distribution of Hu-immunoreactive cells (red) in normal and injured mice. The central lesion area was devoid of Hu-positive neurons. **G–I:** Mac-1 (CD11b)-immunoreactive cells were almost negative in the normal axial section (G), but they were aggregated mainly in the connective tissue scar area in injured spinal cord (H,I). A, B, D, E, G, and H, axial sections; C, F, and I, sagittal sections. Scale bars = 400 μm.

Behavioral Recovery

Given the histopathological improvements, such as the decreased astrogliosis and inflammatory cell infiltration, we investigated whether the histological changes were associated with better functional recovery by using three different behavioral tests. The mice in both the MR-16 group and the control group showed flaccid paralysis with no or little hindlimb movement throughout the first week after SCI, and this was followed by some recovery of hindlimb movement. To assess such functional recovery, we first examined a standardized open-field measure of locomotor function after the SCI, the BBB score, in which 21 is normal function and 0 is bilateral total paralysis of the hindlimbs. When BBB scoring is applied to mice, the size and speed of the hindpaws make it difficult to assign a precise score if the score exceeds 13 points (Ma et al., 2001), but that was not a problem in this study, because none of the mice had scores over 13 points (Jakeman et al., 2000). By 6 weeks after the injury, mice in the MR16-1 group had a significantly higher motor score (9.1 ± 0.5) than the control animals (6.4 ± 0.7), and the differences between the two groups 5 and 6 weeks after the injury were statistically significant (Fig. 7A). In the BBB score, 9 points represents the ability for hindlimb weight bearing. Even in mice, the difference of 8 points and 9 points was clearly detectable, because it was obvious whether they could bear weight or not.

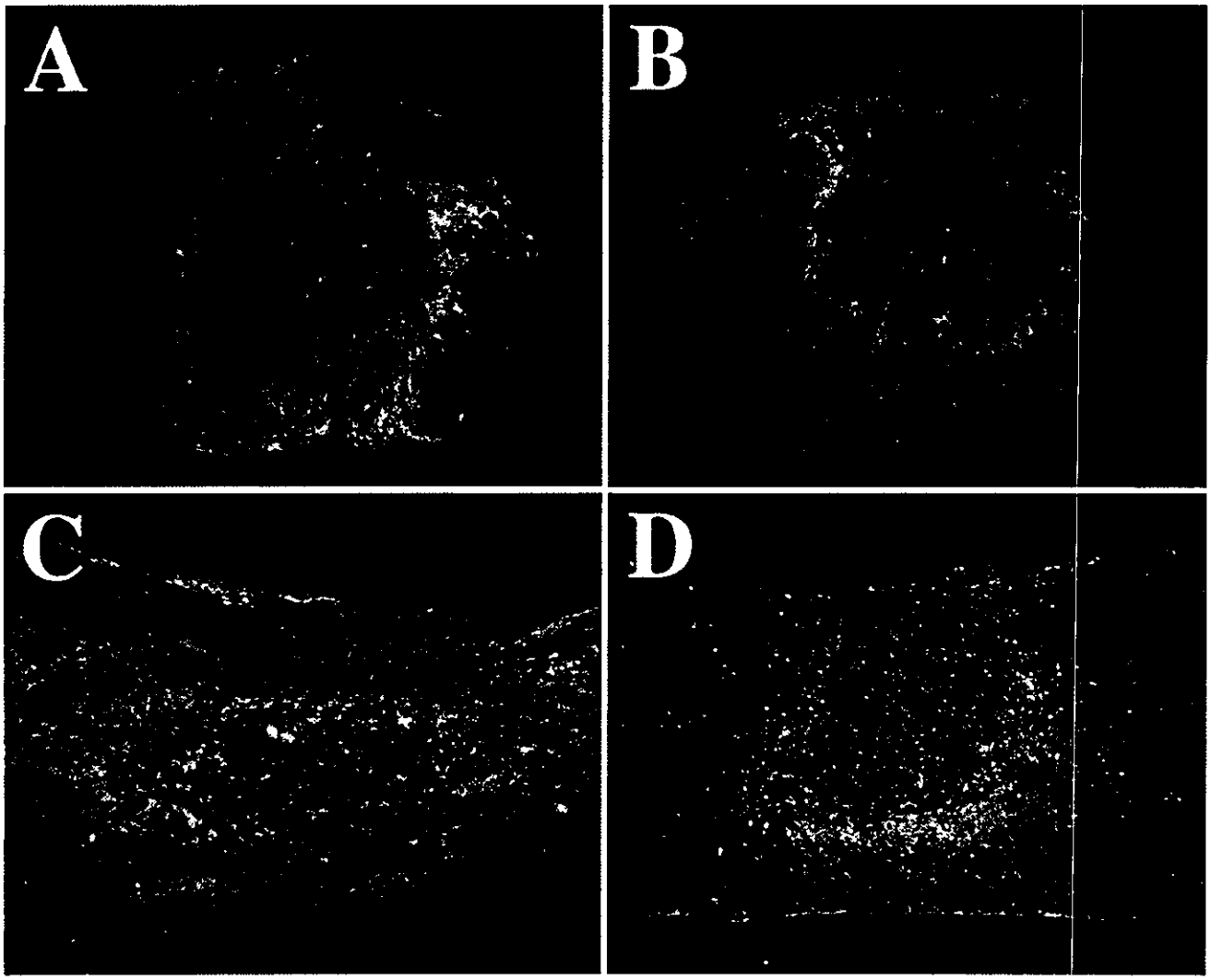

Fig. 3. Sections from the lesion epicenter of control mice (**A,C**) and MR16-1-treated mice (**B,D**) were counterstained with GFAP (green) and BrdU (red). The connective tissue scar area was almost completely GFAP negative but was surrounded with GFAP-positive astrocytes. This area in MR16-1-treated mice was smaller and astrogliosis around the central lesion was suppressed moderately compared with the control mice. A, B, axial sections; C, D, sagittal sections.

We then used a second assay employing SCANET, an automated motion-analysis system for measuring spontaneous motor activity (Shimosato and Ohkuma, 2000; Mikami et al., 2002), which is capable of assessing not only horizontal but also vertical movement. Vertical movement is an adequate index for assessment of locomotor function in spinal cord-injured mice. Mikami et al. (2002) even reported a statistically significant positive correlation between the RG score and the BBB Scale score. The vertical movement analysis revealed that 12 of the 15 mice in the MR16-1 group were able to rear more than once, whereas only 3 of the 15 mice were able to do so in the control group. The difference between the two groups was significant according to Fisher's exact probability test ($P < .05$). However, there were no significant differences in horizontal movements between the groups.

We performed the Rota-rod treadmill test to assess recovery of forelimb–hindlimb coordination. At low speed (5 rpm), there were statistically significant differences between the groups in average and maximum retention time in three trials at 5 and 6 weeks after the injury (Fig. 6B), but no differences were demonstrated at the middle speed (10 rpm) or high speed (15 rpm). These findings indicated that the recovery of forelimb–hindlimb coordination was poor even in the MR16-1 group, and they were consistent with the BBB scores, which never exceeded 12 points. In conclusion, MR16-1 group exhibited better functional recovery than the control mice in all three behavioral evaluations.

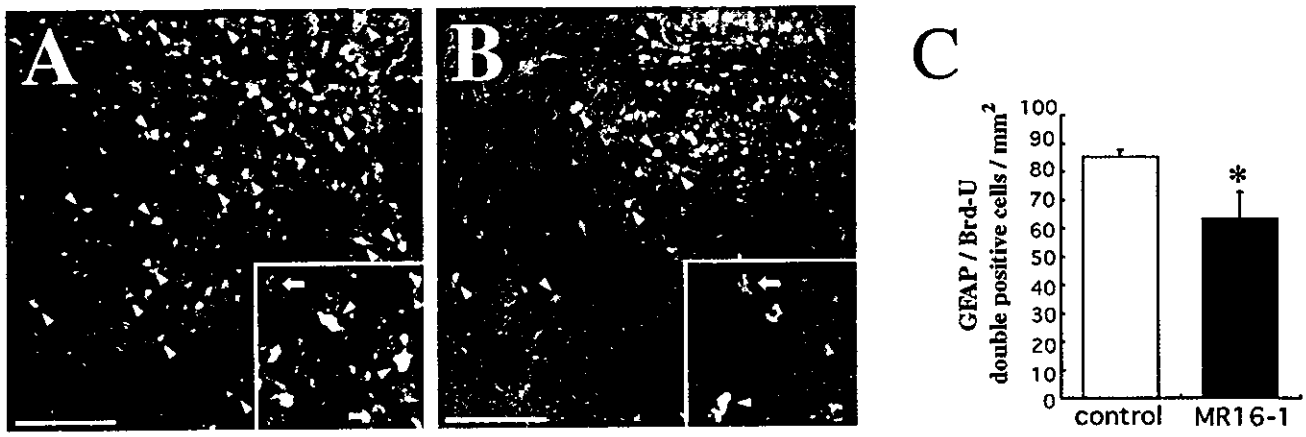

Fig. 4. MR16-1 suppressed the astrogliosis after SCI. **A,B:** Immunofluorescence staining for GFAP (green) and BrdU (red) at 2 weeks after the injury. Confocal imaging of the lesioned area with higher magnification in the control group (A) and MR16-1 group (B). **Insets:** Magnified views of A and B. Arrowheads point to a GFAP and BrdU double-positive cell, and the arrows point to GFAP-positive and BrdU-negative cells. **C:** Quantitative analysis of the average density of GFAP and BrdU double-positive cells at the lesion epicenter and 0.5 mm and 1.0 mm rostral and caudal to the epicenter in both groups. Values are means ± SEM. $*P < .05$; two-tailed t-test (n = 4 in the control group; n = 3 in the MR16-1 treated group). Scale bars = 40 μm.

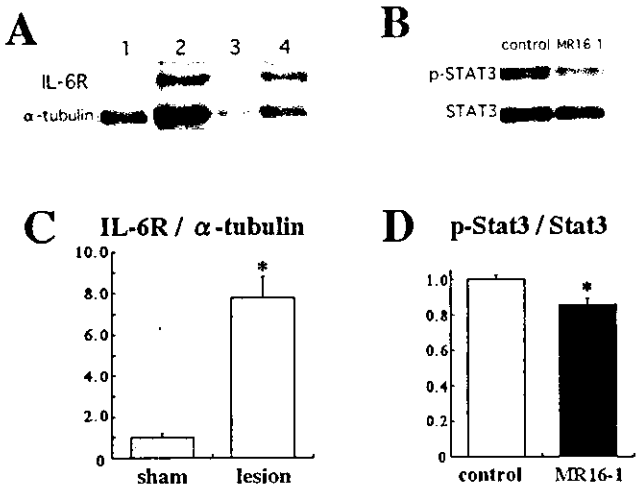

Fig. 5. Western blot analysis. **A,C:** Western blotting of soluble IL-6 receptor in the sham-operated spinal cord (lanes 1, 3) and lesioned spinal cord at 12 hr after the injury (lanes 2, 4). Quantification analysis revealed that the expression of IL-6R was 7.8-fold higher in the lesioned group at 12 hr after the injury compared with that in the sham group (n = 4 per each group). The average expression in the sham group was set as 1.0. $*P < .01$. **B,D:** The phosphorylated-STAT3 expression level in the spinal cord at 12 hr after the injury was quantitatively compared by Western blot analysis. The expression level of phosphorylated STAT3 in the MR16-1-treated group was 85.1% less compared with that in the control group. Values represent means ± SEM of the p-STAT3/STAT3 ratios (n = 4 per each group), with the average ratio in the control group set as 1.0. $*P < .05$.

DISCUSSION

Neutralization of soluble IL-6 receptor (sIL-6R) represents an attractive option for the treatment of several diseases characterized by excessive expression of IL-6, including B-cell neoplasia, rheumatoid arthritis, and autoimmune diseases (Yoshizaki et al., 1989; Takagi et al., 1998; Atreya et al., 2000). In this study, we first showed that the monoclonal anti-IL-6 receptor-α antibody MR16-1 blocked the IL-6 signaling that induced NSPCs to differentiate into astrocytes in vitro. Bonni et al. (1997) observed that activation of the gp130 signaling pathway selectively enhanced the differentiation of embryonic cerebral cortical precursor cells toward astrocytes, and we confirmed very similar effects of IL-6 signaling on NSPCs harvested from the spinal cord of adult mice.

Johansson et al. (1999) demonstrated that the endogenous NSPCs of adult spinal cord proliferate rapidly and differentiate exclusively into astrocytes in response to injury. Although the precise mechanism of this restrictive differentiation of NSPCs remains to be elucidated, activation of IL-6 signaling could be one of the major contributions of such selective astrocytic differentiation after SCI. IL-6 expression increases dramatically during the acute phase of SCI and then declines sharply within a few days (Hostettler and Carlson, 2002; Pan et al., 2002; Nakamura et al., 2003), and we confirmed the increase in sIL-6R (Yan et al., 1992) after SCI by Western blot analysis (Fig. 5A,C). This up-regulation of IL-6 signaling in the acute phase would be closely associated with glial scar formation after SCI (for review see Okano, 2002; Okano et al., 2003). Klein et al. (1997) show a massive reduction in the number of activated GFAP-positive astrocytes when the facial nerve of IL-6-deficient mice was transected, and Brunello et al. (2000) demonstrated massive reactive gliosis with numerous GFAP-immunoreactive astrocytes in all parts of the CNS in uninjured IL-6/sIL-6R double-transgenic mice. Therefore, we hypothesized that the astrogliosis could be suppressed by blocking IL-6 signaling after

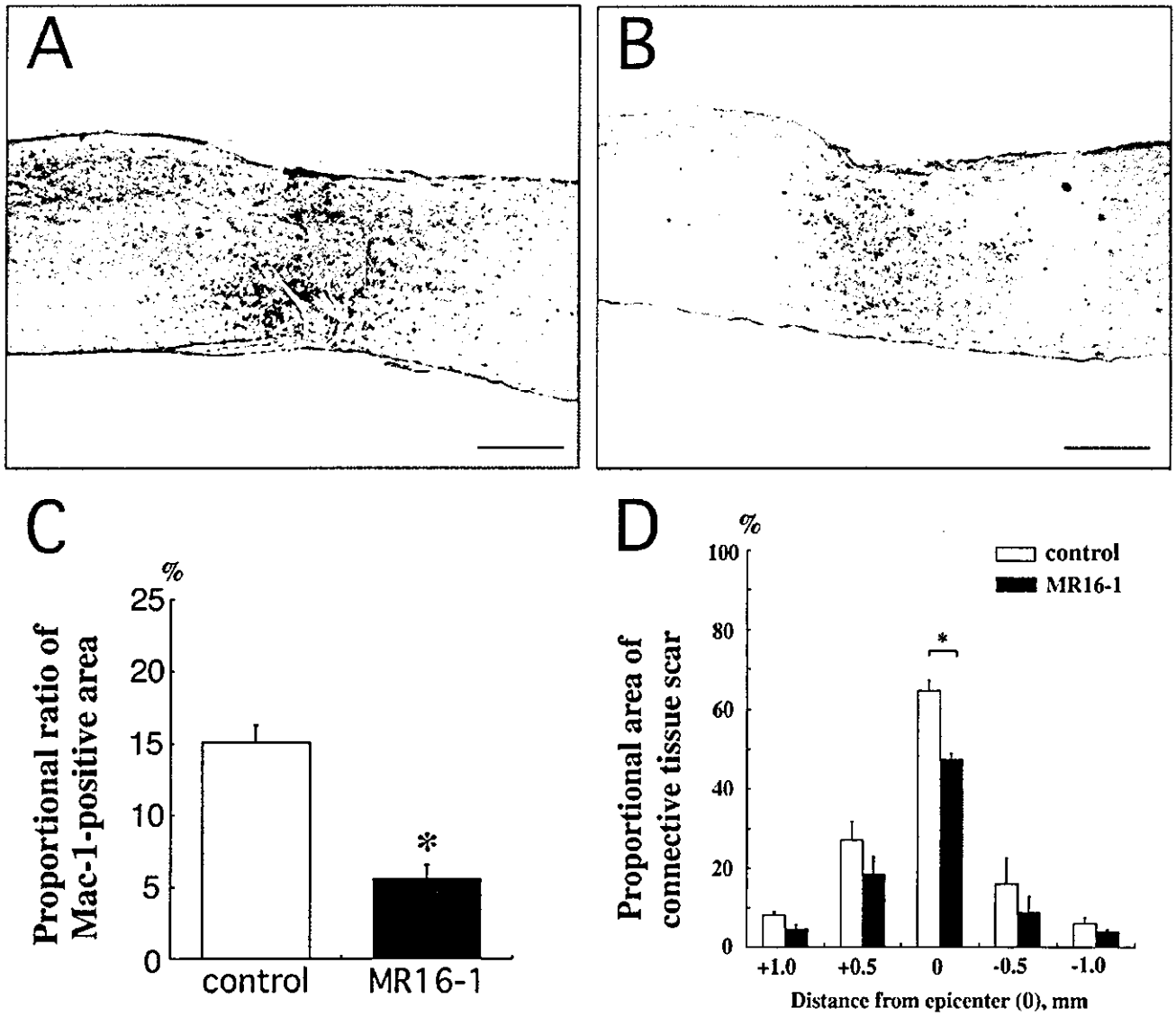

Fig. 6. Inflammatory responses were markedly decreased by MR16-1. **A,B:** Immunolabeling of Mac-1-positive cells in injured spinal cord at 2 weeks after injury. Representative sagittal section at the lesion epicenter from the control group (A) and the M16-1 group (B). **C:** Measurement of the area of Mac-1 immiunoreactivity in 3-mm sagittal sections from both groups. The immunolabeled area was significantly smaller in the MR16-1 group than in the control group. Values are means ± SEM. $*P < .05$; two-tailed t-test (n = 4 in the control group; n = 3 in the MR16-1 group). **D:** The area of the connective tissue scar as a percentage of the total axial area was calculated at the lesion epicenter and 0.5 and 1.0 mm rostral and caudal to the epicenter in both groups. The connective tissue scar area in the epicenter was significantly smaller in the MR16-1 mice. Values are means ± SEM. $*P < .05$; two-tailed t-test (n = 4 per each group). Scale bars = 500 μm.

SCI in vivo. In the present study, we showed a 15% decrease of phosphorylated-STAT3 expression at 12 hr after the injury and a 25% decrease in the number of GFAP and BrdU double-positive cells at 2 weeks after injury with systemic administration of MR16-1, compared with the control animals, suggesting that astrogliosis and IL-6 signaling are closely related. However, the precise mechanism regulating astrogliosis remains to be elucidated. In the present study, we were not able to determine the extent to which endogenous multipotential progenitors or resident astrocytes contributed to the $GFAP^+/BrdU^+$ cells. Kernie et al. (2001), however, reported that a significant amount of the astrogliotic scar formed after an injury is attributable to newly generated astrocytes and not to activation or migration of resident astrocytes.

Glial scar formation is considered a major cause of the poor regeneration after adult CNS after injury. A

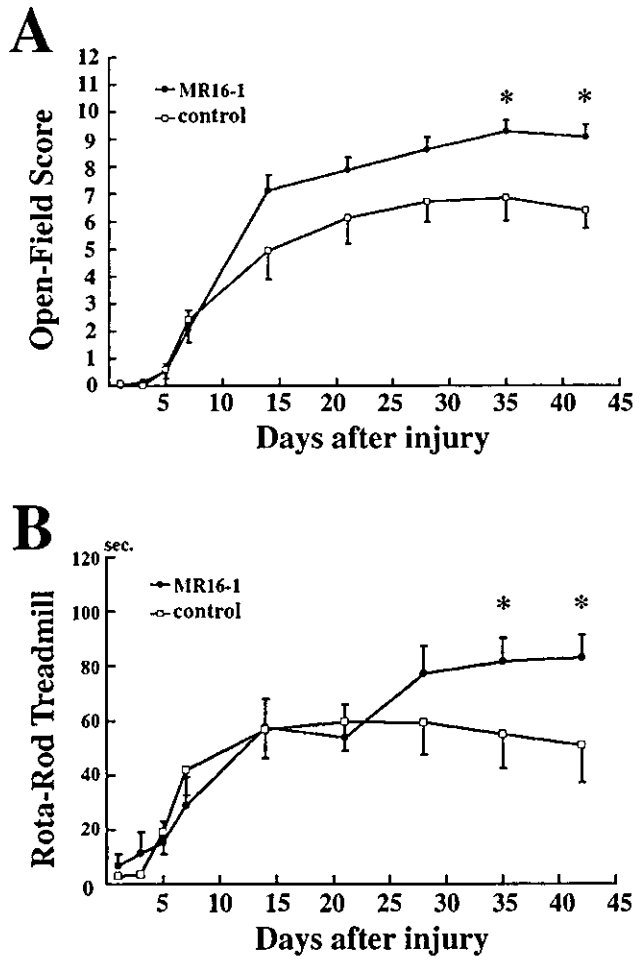

Fig. 7. Effect of MR16-1 on functional recovery. **A:** BBB scores in the control group (n = 15) and MR16-1 group (n = 15) were evaluated over a 6-week period. **B:** Retention time on the rotating rod in the control group (n = 15) and MR16-1 group (n = 15) at a speed of 5 rpm. Squares represent control mice, and circles represent MR16-1-treated mice. Values are means ± SEM. $*P < .05$; two-tailed *t*-test.

recent study reported that glial scars and associated extracellular matrix inhibit axonal regeneration with several molecules, such as chondroitin sulfate proteoglycans, tenascin, brevican, and neurocan (Fawcett and Asher, 1999). Bradbury et al. (2002) also demonstrated that degradation of chondroitin sulfate proteoglycans that are contained in glial scars at injury site with chondroitinase ABC improved functional recovery and promoted regeneration of both ascending sensory projections and descending long tract axons. Thus, modulating astrogliosis is a rational target for treating spinal cord injury and enhancing axonal regeneration, resulting in functional recovery (McGraw et al., 2001). Ridet et al. (2000) reported that suppression of glial scar formation with a 2-Gy dose of radiation after injury also improved functional recovery. In the present study, we demonstrated that administration of MR16-1 promoted functional recovery in three different behavioral evaluations (Fig. 7). Although further investigations are required, one possible explanation for the observed functional recovery is that the suppression of astrogliosis by MR16-1 treatment reduced the expression of glial scar-derived inhibitory molecules against axonal regeneration, which promoted axonal regeneration after injury.

Manipulation of inflammatory responses is another therapeutic strategy for SCI. Although the precise functions and effects of inflammatory cells after injury have not been completely elucidated, previous studies have suggested that inflammatory responses spread the damage to surrounding tissue, induce apoptotic cell death, and impair spontaneous regeneration and functional recovery (Carlson et al., 1998; Popovich and Jones, 2003). Several approaches to protecting the injured spinal cord from secondary pathological processes, such as the antiinflammatory cytokine IL-10, erythropoietin, matrix metalloprotease inhibitor, and methylprednisolone, have been assessed and been demonstrated to be effective, even in terms of functional recovery (Bracken et al., 1997; Bethea et al., 1999; Gorio et al., 2002; Nobel et al., 2002). IL-6 is one of the principal proinflammatory cytokines; it plays roles in regulating various steps in inflammatory reactions, i.e., activation and infiltration by neutrophils, monocytes, macrophages, and lymphocytes (Van Wagoner and Benveniste, 1999; Leskovar et al., 2000). The number of inflammatory cells is significantly correlated with the amount of tissue damage at each level (Carlson et al., 1998), and the size of the CTS, which is the characteristic lesion of contusive SCI in mice, as opposed to central cavitation in rats, correlates with the severity of the injury (Ma et al., 2001). We tested, based on these studies, our hypothesis that MR16-1 would suppress the inflammatory response after injury by assessing the extent of Mac-1-positive inflammatory cell infiltration and measuring the area of the CTS. The results demonstrated that fewer Mac-1-positive cells infiltrated both the gray and the white matter and that the CTS area at the lesion epicenter was significantly smaller in the MR16-1 group than in the control group (Fig. 6). This modulation of the inflammatory response after injury by administration of MR16-1 probably attenuated the tissue damage and secondary neural destruction and caused the functional recovery demonstrated in the present study (Fig. 7). Our findings are consistent with the results of previous studies suggesting that administration of proinflammatory cytokines at lesion sites 1 day after an injury increases the recruitment and activation of macrophages, neutrophils, and microglial cells (Klusman and Schwab, 1997) and that delivery of IL-6/sIL-6R fusion protein to injury sites induces a sixfold increase in neutrophils and a twofold increase of macrophages and microglial cells (Lacroix et al., 2002).

By contrast, IL-6 exerts multiple effects in the CNS, and several experiments have shown the neuronal protective and outgrowth effects of IL-6 signaling. For example, Marz et al. (1998) showed that IL-6 signaling enhances neuronal survival in rat sympathetic neurons, and Hirota et

al. (1996) observed accelerated regeneration of the axotomized hypoglossal nerve in transgenic mice constitutively expressing IL-6 and IL-6R. Administration of IL-6 to animals with cerebral ischemia reduced tissue damage and prevented learning disabilities in vivo (Matsuda et al., 1996; Loddick et al., 1998). In SCI, however, delivery of IL-6/sIL-6R fusion protein (hyper-IL-6) to the lesion site induced a fourfold decrease in axonal outgrowth, which indicated that the neurotrophic effects of IL-6 were overwhelmed by its proinflammatory features in vivo (Lacroix et al., 2002). These clear differences in IL-6 effect may depend on the level and timing of its expression. Although the role of IL-6 signaling seemed to be complex and well regulated in accordance with the physiopathology, we wish to emphasize the neurotoxic effect of IL-6, at least in the acute phase after SCI. We also confirmed by ELISA (data not shown) that the half-life of MR16-1 is about 3 days in injured mice, so the kinetics of MR16-1 would produce an ideal effect, because it suppresses excess IL-6 signaling only in the acute phase and dose not interfere the neuroprotective effect in the subacute and chronic phases.

A critical merit of this sIL-6R antibody is that humanized antibody to human IL-6R (MRA; Atlizumab) has already been reshaped (Sato et al., 1993), and its therapeutic efficacy has been confirmed in clinical trials in several diseases, including rheumatoid arthritis, Castleman's disease, and multiple myeloma (Sato et al., 1993; Nishimoto et al., 2000; Choy et al., 2002). The Phase II clinical trial in rheumatoid arthritis has already been completed in Japan and Europe, and safety, tolerability, antigenicity, pharmacokinetics, and efficacy have been demonstrated. Although the data reported here are preliminary, they suggest that blockage of IL-6 signaling may be beneficial in patients with acute SCI. In summary, the results of this study show that a single dose of anti-mouse IL-6R monoclonal antibody enhances functional recovery after SCI in adult mice, probably by attenuating inflammatory response, secondary tissue damage, and astrogliosis.

ACKNOWLEDGMENTS

We thank Drs. K. Shiba and T. Ueta (Spina Cord Injury Center, Fukuoka, Japan) for their continuous encouragement and valuable discussions. This work was supported by grants from the Japanese Ministry of Education, Culture, Sports, Science and Technology and the Japan Science and Technology Corporation (CREST) to H.O., and a Grant-in-Aid for the 21st Century COE (Center of Excellence) program to Keio University from the Japanese Ministry of Education, Culture, Sports, Science and Technology.

REFERENCES

Atreya R, Mudter J, Finotto S, Mullberg J, Jostock T, Wirtz S, Schutz M, Bartsch B, Holtmann M, Becker C, Strand D, Czaja J, Schlaak JF, Lehr HA, Autschbach F, Schurmann G, Nishimoto N, Yoshizaki K, Ito H, Kishimoto T, Galle PR, Rose-John S, Neurath MF. 2000. Blockade of interleukin 6 trans signaling suppresses T-cell resistance against apoptosis in chronic intestinal inflammation: evidence in crohn disease and experimental colitis in vivo. Nat Med 6:583–588.

Basso DM, Beattie MS, Bresnahan JC. 1996. Graded histological and locomotor outcomes after spinal cord contusion using the NYU weight-drop device versus transection. Exp Neurol 139:244–256.

Bethea JR, Nagashima H, Acosta MC, Briceno C, Gomez F, Marcillo AE, Loor K, Green J, Dietrich WD. 1999. Systemically administered interleukin-10 reduces tumor necrosis factor-alpha production and significantly improves functional recovery following traumatic spinal cord injury in rats. J Neurotrauma 16:851–863.

Bjorklund A, Lindvall O. 2000. Self-repair in the brain. Nature 405:892–895.

Bonni A, Sun Y, Nadal-Vicens M, Bhatt A, Frank DA, Rozovsky I, Stahl N, Yancopoulos GD, Greenberg ME. 1997. Regulation of gliogenesis in the central nervous system by the JAK-STAT signaling pathway. Science 278:477–483.

Bracken MB, Shepard MJ, Holford TR, Leo-Summers L, Aldrich EF, Fazl M, Fehlings M, Herr DL, Hitchon PW, Marshall LF, Nockels RP, Pascale V, Perot PL Jr, Piepmeier J, Sonntag VK, Wagner F, Wilberger JE, Winn HR, Young W. 1997. Administration of methylprednisolone for 24 or 48 hr or tirilazad mesylate for 48 hr in the treatment of acute spinal cord injury. Results of the Third National Acute Spinal Cord Injury Randomized Controlled Trial. National Acute Spinal Cord Injury Study. JAMA 277:1597–1604.

Bradbury EJ, Moon LD, Popat RJ, King VR, Bennett GS, Patel PN, Fawcett JW, McMahon SB. 2002. Chondroitinase ABC promotes functional recovery after spinal cord injury. Nature 416:636–640.

Brunello AG, Weissenberger J, Kappeler A, Vallan C, Peters M, Rose-John S, Weis J. 2000. Astrocytic alterations in interleukin-6/soluble interleukin-6 receptor alpha double-transgenic mice. Am J Pathol 157: 1485–1493.

Carlson SL, Parrish ME, Springer JE, Doty K, Dossett L. 1998. Acute inflammatory response in spinal cord following impact injury. Exp Neurol 151:77–88.

Choy EH, Isenberg DA, Garrood T, Farrow S, Ioannou Y, Bird H, Cheung N, Williams B, Hazleman B, Price R, Yoshizaki K, Nishimoto N, Kishimoto T, Panayi GS. 2002. Therapeutic benefit of blocking interleukin-6 activity with an anti-interleukin-6 receptor monoclonal antibody in rheumatoid arthritis: a randomized, double-blind, placebo-controlled, dose-escalation trial. Arthritis Rheum 46:3143–3150.

David S, Lacroix S. 2003. Molecular approaches to spinal cord repair. Annu Rev Neurosci 26:411–440.

Fawcett JW, Asher RA. 1999. The glial scar and central nervous system repair. Brain Res Bull 49:377–391.

Gorio A, Gokmen N, Erbayraktar S, Yilmaz O, Madaschi L, Cichetti C, Di Giulio AM, Vardar E, Cerami A, Brines M. 2002. Recombinant human erythropoietin counteracts secondary injury and markedly enhances neurological recovery from experimental spinal cord trauma. Proc Natl Acad Sci USA 99:9450–9455.

Gruner JA. 1992. A monitored contusion model of spinal cord injury in the rat. J Neurotrauma 9:123–128.

Hirota H, Kiyama H, Kishimoto T, Taga T. 1996. Accelerated nerve regeneration in mice by upregulated expression of interleukin (IL) 6 and IL-6 receptor after trauma. J Exp Med 183:2627–2634.

Horner PJ, Power AE, Kempermann G, Kuhn HG, Palmer TD, Winkler J, Thal LJ, Gage FH. 2000. Proliferation and differentiation of progenitor cells throughout the intact adult rat spinal cord. J Neurosci 20:2218–2228.

Hostettler ME, Carlson SL. 2002. PAF antagonist treatment reduces pro-inflammatory cytokine mRNA after spinal cord injury. Neuroreport 13:21–24.

Jakeman LB, Guan Z, Wei P, Ponnappan R, Dzwonczyk R, Popovich PG, Stokes BT. 2000. Traumatic spinal cord injury produced by controlled contusion in mouse. J Neurotrauma 17:299–319.

Johansson CB, Momma S, Clarke DL, Risling M, Lendahl U, Frisen J. 1999. Identification of a neural stem cell in the adult mammalian central nervous system. Cell 96:25–34.

Katsume A, Saito H, Yamada Y, Yorozu K, Ueda O, Akamatsu KI, Nishimoto N, Kishimoto T, Yoshizaki K, Ohsugi Y. 2002. Anti-interleukin 6 (IL-6) receptor antibody suppresses castleman's disease like symptoms emerged in IL-6 transgenic mice. Cytokine 20:304–311.

Kernie SG, Erwin TM, Parada LF. 2001. Brain remodeling due to neuronal and astrocytic proliferation after controlled cortical injury in mice. J Neurosci Res 66:317–326.

Klein MA, Moller JC, Jones LL, Bluethmann H, Kreutzberg GW, Raivich G. 1997. Impaired neuroglial activation in interleukin-6 deficient mice. Glia 19:227–233.

Klusman I, Schwab ME. 1997. Effects of pro-inflammatory cytokines in experimental spinal cord injury. Brain Res 762:173–184.

Kuhn PL, Wrathall JR. 1998. A mouse model of graded contusive spinal cord injury. J Neurotrauma 15:125–140.

Lacroix S, Chang L, Rose-John S, Tuszynski MH. 2003. Delivery of hyper-interleukin-6 to the injured spinal cord increases neutrophil and macrophage infiltration and inhibits axonal growth. J Comp Neurol 454:213–228.

Leskovar A, Moriarty LJ, Turek JJ, Schoenlein IA, Borgens RB. 2000. The macrophage in acute neural injury: changes in cell numbers over time and levels of cytokine production in mammalian central and peripheral nervous systems. J Exp Biol 203:1783–1795.

Loddick SA, Turnbull AV, Rothwell NJ. 1998. Cerebral interleukin-6 is neuroprotective during permanent focal cerebral ischemia in the rat. J Cereb Blood Flow Metab 18:176–179.

Ma M, Basso DM, Walters P, Stokes BT, Jakeman LB. 2001. Behavioral and histological outcomes following graded spinal cord contusion injury in the C57Bl/6 mouse. Exp Neurol 169:239–254.

Marz P, Cheng JG, Gadient RA, Patterson PH, Stoyan T, Otten U, Rose-John S. 1998. Sympathetic neurons can produce and respond to interleukin 6. Proc Natl Acad Sci USA 95:3251–3256.

Matsuda S, Wen TC, Morita F, Otsuka H, Igase K, Yoshimura H, Sakanaka M. 1996. Interleukin-6 prevents ischemia-induced learning disability and neuronal and synaptic loss in gerbils. Neurosci Lett 204:109–112.

McGraw J, Hiebert GW, Steeves JD. 2001. Modulating astrogliosis after neurotrauma. J Neurosci Res 63:109–115.

Meima L, Moran P, Matthews W, Caras IW. 1997. Lerk2 (ephrin-B1) is a collapsing factor for a subset of cortical growth cones and acts by a mechanism different from AL-1 (ephrin-A5). Mol Cell Neurosci 9:314–328.

Mikami Y, Toda M, Watanabe M, Nakamura M, Toyama Y, Kawakami Y. 2002. A simple and reliable behavioral analysis of locomotor function after spinal cord injury in mice. Technical note. J Neurosurg 97:142–147.

Nakamura M, Houghtling RA, McArthur L, Bayer BM, Bregman BS. 2003. Difference in cytokine gene expression profile between acute and secondary injury in adult rat spinal cord. Ex Neurol 184:313–325.

Nakashima K, Yanagisawa M, Arakawa H, Kimura N, Hisatsune T, Kawabata M, Miyazono K, Taga T. 1999. Synergistic signaling in fetal brain by STAT3-Smad1 complex bridged by p300. Science 284:479–482.

Nishimoto N, Sasai M, Shima Y, Nakagawa M, Matsumoto T, Shirai T, Kishimoto T, Yoshizaki K. 2000. Improvement in Castleman's disease by humanized anti-interleukin-6 receptor antibody therapy. Blood 95:56–61.

Noble LJ, Donovan F, Igarashi T, Goussev S, Werb Z. 2002. Matrix metalloproteinases limit functional recovery after spinal cord injury by modulation of early vascular events. J Neurosci 22:7526–7535.

Ogura H, Matsumoto M, Mikoshiba K. 2001. Motor discoordination in mutant mice heterozygous for the type 1 inositol 1,4,5-trisphosphate receptor. Behav Brain Res 122:215–219.

Ohtani T, Ishihara K, Atsumi T, Nishida K, Kaneko Y, Miyata T, Itoh S, Narimatsu M, Maeda H, Fukada T, Itoh M, Okano H, Hibi M, Hirano T. 2000. Dissection of signaling cascades through gp130 in vivo: reciprocal roles for STAT3- and SHP2-mediated signals in immune responses. Immunity 12:95–105.

Okano H. 2002. Stem cell biology of the central nervous system. J Neurosci Res 69:698–707.

Okano H, Ogawa Y, Nakamura M, kaneko S, Iwanami A, Toyama Y. 2003. Transplantation of neural stem cells into the spinal cord after injury. Semin Cell Dev Biol 14:191–198.

Okazaki M, Yamada Y, Nishimoto N, Yoshizaki K, Mihara M. 2002. Characterization of anti-mouse interleukin-6 receptor antibody. Immunol Lett 84:231–240.

Pan JZ, Ni L, Sodhi A, Aguanno A, Young W, Hart RP. 2002. Cytokine activity contributes to induction of inflammatory cytokine mRNAs in spinal cord following contusion. J Neurosci Res 68:315–322.

Popovich PG, Jones TB. 2003. Manipulating neuroinflammatory reactions in the injured spinal cord: back to basics. Trends Pharmacol Sci 24:13–17.

Reynolds BA, Tetzlaff W, Weiss S. 1992. A multipotent EGF-responsive striatal embryonic progenitor cell produces neurons and astrocytes. J Neurosci 12:4565–4574.

Ridet JL, Pencalet P, Belcram M, Giraudeau B, Chastang C, Philippon J, Mallet J, Privat A, Schwartz L. 2000. Effects of spinal cord X-irradiation on the recovery of paraplegic rats. Exp Neurol 161:1–14.

Romano M, Sironi M, Toniatti C, Polentarutti N, Fruscella P, Ghezzi P, Faggioni R, Luini W, van Hinsbergh V, Sozzani S, Bussolino F, Poli V, Ciliberto G, Mantovani A. 1997. Role of IL-6 and its soluble receptor in induction of chemokines and leukocyte recruitment. Immunity 6:315–325.

Sato K, Tsuchiya M, Saldanha J, Koishihara Y, Ohsugi Y, Kishimoto T, Bendig MM. 1993. Reshaping a human antibody to inhibit the interleukin 6-dependent tumor cell growth. Cancer Res 53:851–856.

Shimazaki T, Shingo T, Weiss S. 2001. The ciliary neurotrophic factor/leukemia inhibitory factor/gp130 receptor complex operates in the maintenance of mammalian forebrain neural stem cells. J Neurosci 21:7642–7653.

Shimosato K, Ohkuma S. 2000. Simultaneous monitoring of conditioned place preference and locomotor sensitization following repeated administration of cocaine and methamphetamine. Pharmacol Biochem Behav 66:285–292.

Taga T, Kishimoto T. 1997. Gp130 and the interleukin-6 family of cytokines. Annu Rev Immunol 15:797–819.

Taga T, Hibi M, Hirata Y, Yamasaki K, Yasukawa K, Matsuda T, Hirano T, Kishimoto T. 1989. Interleukin-6 triggers the association of its receptor with a possible signal transducer, gp130. Cell 58:573–581.

Takagi N, Mihara M, Moriya Y, Nishimoto N, Yoshizaki K, Kishimoto T, Takeda Y, Ohsugi Y. 1998. Blockage of interleukin-6 receptor ameliorates joint disease in murine collagen-induced arthritis. Arthritis Rheum 41:2117–2121.

Takahashi M, Arai Y, Kurosawa H, Sueyoshi N, Shirai S. 2003. Ependymal cell reactions in spinal cord segments after compression injury in adult rat. J Neuropathol Exp Neurol 62:185–194.

Tamura T, Udagawa N, Takahashi N, Miyaura C, Tanaka S, Yamada Y, Koishihara Y, Ohsugi Y, Kumaki K, Taga T. 1993. Soluble interleukin-6 receptor triggers osteoclast formation by interleukin 6. Proc Natl Acad Sci USA 90:11924–11928.

Tuna M, Polat S, Erman T, Ildan F, Gocer AI, Tuna N, Tamer L, Kaya M, Cetinalp E. 2001. Effect of anti-rat interleukin-6 antibody after spinal cord injury in the rat: inducible nitric oxide synthase expression, sodium- and potassium-activated, magnesium-dependent adenosine-5'-triphosphatase and superoxide dismutase activation, and ultrastructural changes. J Neurosurg 95:64–73.

Van Wagoner NJ, Benveniste EN. 1999. Interleukin-6 expression and regulation in astrocytes. J Neuroimmunol 100:124–139.

Yan HQ, Banos MA, Herregodts P, Hooghe R, Hooghe-Peters EL. 1992. Expression of interleukin (IL)-1 beta, IL-6 and their respective receptors in the normal rat brain and after injury. Eur J Immunol 22:2963–7291.

THE JOURNAL OF BIOLOGICAL CHEMISTRY
Vol. 278, No. 31, Issue of August 1, pp. 29106–29114, 2003
Printed in U.S.A.

Dorfin Localizes to Lewy Bodies and Ubiquitylates Synphilin-1*

Received for publication, March 18, 2003, and in revised form, May 12, 2003
Published, JBC Papers in Press, May 15, 2003, DOI 10.1074/jbc.M302763200

Takashi Ito, Jun-ichi Niwa‡, Nozomi Hishikawa, Shinsuke Ishigaki, Manabu Doyu, and Gen Sobue§

From the Department of Neurology, Nagoya University Graduate School of Medicine, Showa-ku, Nagoya 466-8550, Japan

Parkinson's disease (PD) is a neurodegenerative disease characterized by loss of nigra dopaminergic neurons. Lewy bodies (LBs) are a characteristic neuronal inclusion in PD brains. In this study, we report that Dorfin, a RING finger-type ubiquityl ligase for mutant superoxide dismutase-1, was localized with ubiquitin in LBs. Recently, synphilin-1 was identified to associate with α-synuclein and to be a major component of LBs. We found that overexpression of synphilin-1 in cultured cells led to the formation of large juxtanuclear inclusions, but showed no cytotoxicity. Dorfin colocalized in these large inclusions with ubiquitin and proteasomal components. In contrast to full-length synphilin-1, overexpression of the central portion of synphilin-1, including ankyrin-like repeats, a coiled-coil domain, and an ATP/GTP-binding domain, predominantly led to the formation of small punctate aggregates scattered throughout the cytoplasm and showed cytotoxic effects. Dorfin and ubiquitin did not localize in these small aggregates. Overexpression of the N or C terminus of synphilin-1 did not lead to the formation of any aggregates. Dorfin physically bound and ubiquitylated synphilin-1 through its central portion, but did not ubiquitylate wild-type or mutant α-synuclein. These results suggest that the central domain of synphilin-1 has an important role in the formation of aggregates and cytotoxicity and that Dorfin may be involved in the pathogenic process of PD and LB formation by ubiquitylation of synphilin-1.

Parkinson's disease (PD)[1] is a neurodegenerative disease caused by loss of nigra dopaminergic neurons. Lewy bodies (LBs) are a characteristic neuronal inclusion in PD brains (1–4). Although LBs are a prominent pathological feature of PD, the underlying molecular mechanism accounting for LB formation is poorly understood. Several lines of evidence have suggested that derangements in the ubiquitin/proteasome protein degradation pathway play a prominent role in the pathogenesis of PD (5). Ubiquitin and proteasome subunits colocalize in LBs (6, 7), and biochemical studies have revealed reduced catalytic activities of proteasomes in the lesions of PD (8, 9). The gene product responsible for autosomal recessive juvenile parkinsonism, parkin (10), is an E3 ubiquityl ligase (11–13). Accumulation of target protein(s) due to loss of the ubiquitylation function of parkin may contribute to the development of autosomal recessive juvenile parkinsonism. In addition, a missense mutation in UCHL1 (ubiquitin C-terminal hydrolase L1) has been described in a family with PD (14). UCHL1 produces monomeric ubiquitin by cleaving polyubiquitin chains (15). Recently, ubiquityl ligase activity as well as the hydrolase activity of UCHL1 were also reported (16).

α-Synuclein is a 19-kDa presynaptic vesicular protein of unconfirmed function and one of the major components of LBs (17, 18). Mutations in α-synuclein (A30P and A53T) cause a rare autosomal dominant form of PD, which shares many phenotypic characteristics with sporadic PD (19, 20). α-Synuclein aggregates deposit in LBs in both autosomal dominant and sporadic forms of PD (21, 22). In addition, it has been reported that transgenic flies and mice overexpressing human wild-type or mutant α-synuclein have abnormal cellular accumulation of α-synuclein and neuronal dysfunction and degeneration (23–30), indicating that α-synuclein has a role in the pathogenesis of both familial and sporadic forms of PD.

Synphilin-1 was identified recently by yeast two-hybrid techniques as a novel protein that interacts with α-synuclein (31). α-Synuclein amino acids 1–65 are is sufficient for interaction, and the central portion of synphilin-1 (amino acids 349–555) is necessary and sufficient for interaction with α-synuclein (32). It has also been reported that the C terminus of α-synuclein is closely associated with the C terminus of synphilin-1 and that a weak interaction occurs between the N terminus of α-synuclein and synphilin-1 (33). Synphilin-1 is highly concentrated in presynaptic nerve terminals, and its association with synaptic vesicles is modulated by α-synuclein (34). Coexpression of α-synuclein and synphilin-1 in transfected cells results in the formation of eosinophil cytoplasmic inclusions that resemble LBs (31, 35), whereas transfection of synphilin-1 alone without expression of α-synuclein or parkin can also produce cytoplasmic inclusions in cultured cells (36, 37). Furthermore, synphilin-1 is ubiquitylated and degraded by proteasomes in human embryonic kidney 293 (HEK293) cells (37) and is localized as another major component of LBs in the brains of patients with PD (38, 39). Thus, the process through which aggregations are formed by synphilin-1 may be important in the pathogenesis of PD.

Dorfin is a gene product (which we cloned from anterior horn tissues of human spinal cord) (40) that contains a RING finger/IBR (in between RING finger) motif (41) at its N terminus. It was reported that HHARI (human homologue of ariadne) and H7-AP1 (UbcH7-associated protein-1), both RING finger/IBR

* This work was supported in part by a Center of Excellence grant from the Ministry of Education, Culture, Sports, Science, and Technology and by grants from the Ministry of Health, Labor, and Welfare of Japan. The costs of publication of this article were defrayed in part by the payment of page charges. This article must therefore be hereby marked "*advertisement*" in accordance with 18 U.S.C. Section 1734 solely to indicate this fact.

‡ Research Fellow of the Japan Society for the Promotion of Science for Young Scientists.

§ To whom correspondence should be addressed: Dept. of Neurology, Nagoya University Graduate School of Medicine, 65 Tsurumai-cho, Showa-ku, Nagoya 466-8550, Japan. Tel.: 81-52-744-2385; Fax: 81-52-744-2384; E-mail: sobueg@med.nagoya-u.ac.jp.

[1] The abbreviations used are: PD, Parkinson's disease; LBs, Lewy bodies; E1, ubiquitin-activating enzyme; E2, ubiquitin carrier protein; E3, ubiquitin-protein isopeptide ligase; HEK293, human embryonic kidney 293; ALS, amyotrophic lateral sclerosis; SOD1, superoxide dismutase-1; IP, immunopurified; MTS, 3-(4,5-dimethylthiazol-2-yl)-5-(3-carboxymethoxyphenyl)-2-(4-sulfophenyl)-2*H*-tetrazolium, inner salt.

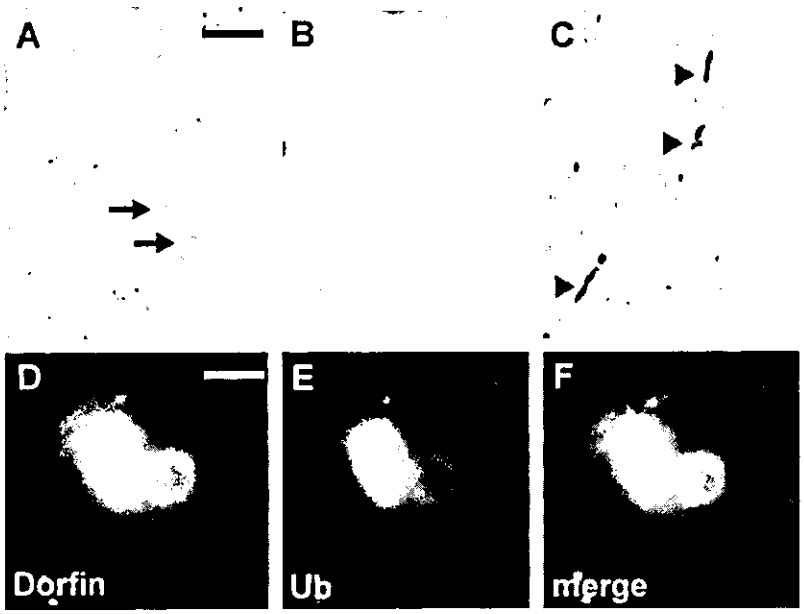

FIG. 1. **Colocalization of Dorfin and ubiquitin in LBs of PD.** Substantia nigra tissue of PD cases was immunohistochemically stained with anti-Dorfin antibody. *A*, LBs (*arrows*) in neurons were strongly stained. *B*, the peripheral rim of a typical LB was predominantly stained with anti-Dorfin antibody. *C*, Lewy neurites (*arrowheads*) were also Dorfin-immunoreactive. The *scale bar* in *A* is equivalent to 100 μm in *A* and *C* and 12 μm in *B*. *D–F*, shown are laser scanning confocal microscopy images of double-labeling immunofluorescence study of LB. Frozen sections prepared from substantia nigra tissue of PD were incubated with rabbit anti-Dorfin IgG and labeled with Alexa Fluor 568-conjugated anti-rabbit antibodies (*red* in *D*) and mouse monoclonal anti-ubiquitin and Alexa Fluor 488-conjugated anti-mouse antibodies (*green* in *E*). *F* shows a merged image of the double-stained LB (*D* and *E*), and regions of overlap between Dorfin and ubiquitin immunoreactivities are shown in *yellow*. The *scale bar* in *D* is equivalent to 10 μm and also applies to *E* and *F*.

motif-containing proteins, interact with the ubiquitin carrier protein (E2) UbcH7 through the RING finger/IBR motif and that a distinct subclass of RING finger/IBR motif-containing proteins represents a new family of proteins that specifically interact with distinct E2 enzymes (42, 43). Dorfin is a juxtanuclearly located E3 ubiquityl ligase and may function in the microtubule-organizing centers (40). In the spinal cords of patients with sporadic and familial forms of amyotrophic lateral sclerosis (ALS) with an SOD1 mutation, Dorfin is colocalized with ubiquitin in hyaline inclusions (44). Dorfin physically binds and ubiquitylates various SOD1 mutants derived from familial ALS patients and enhances their degradation (44). Thus, an important and interesting question is whether Dorfin is colocalized with ubiquitin in LBs of PD.

In this study, we show that Dorfin is colocalized with ubiquitin in LBs of PD. We found that Dorfin ubiquitylates synphilin-1 and that overexpression of synphilin-1 leads to ubiquitylated inclusions resembling LBs in cultured cells.

EXPERIMENTAL PROCEDURES

Immunohistochemistry—Immunohistochemical studies were carried out on 20% buffered, Formalin-fixed, paraffin-embedded autopsied brains filed in the Department of Neurology of the Nagoya University Graduate School of Medicine. Five PD brains (67–69 years of age, four men and one woman) and five controls without neurological disease (61–78 years of age, four men and one woman) were studied. The diagnosis of all cases was confirmed by clinical and pathological criteria. Immunohistochemistry was performed as described previously (45). Rabbit polyclonal antiserum was raised against a C-terminal portion of Dorfin (amino acid 678–690) as described previously (40). Dorfin antiserum (1:200 dilution) and monoclonal anti-ubiquitin antibody (P4D1, 1:400 dilution; Santa Cruz Biotechnology) were used. To assess the colocalization of Dorfin and ubiquitin, a double-labeling immunofluorescence study was performed on selected sections with a combination of anti-Dorfin and anti-ubiquitin antibodies. Anti-Dorfin antibody was visualized by goat anti-rabbit IgG coupled with Alexa Fluor 568 (Molecular Probes, Inc.), and anti-ubiquitin antibody was visualized with sheep anti-mouse IgG coupled with Alexa Fluor 488 (Molecular Probes, Inc.) and observed under a Carl Zeiss LSM-510 laser scanning confocal microscope. For cultured cells, immunostaining was performed as follows. COS-7 cells transiently expressing synphilin-1-DsRed fusion protein in a 4-chamber slide (Nalge Nunc) coated with rat tail collagen (Roche Diagnostics) were fixed with methanol at −20 °C for 10 min, air-dried, and blocked with 5% goat serum for 30 min. Cells were then incubated overnight at 4 °C with the appropriate primary antibody diluted in phosphate-buffered saline. After washing three times with phosphate-buffered saline, Alexa Fluor 488-conjugated secondary antibody (1:1000 dilution; Molecular Probes, Inc.) was added for 1 h at room temperature. Samples were visualized under an Olympus BX51 epifluorescence microscope. Primary antibodies against ubiquitin (P4D1, 1:200 dilution), Hsp70 (heat shock protein of 70 kDa; 1:5000 dilution; Stressgen Biotech Corp.), the 20 S proteasome core subunit (1:5000 dilution; Affiniti), and UbcH7 (1:100 dilution; Transduction Laboratories) were used.

Expression Plasmids, Cell Culture, and Transfection—Human synphilin-1 cDNA containing the entire coding region was amplified by *Pfu* Turbo DNA polymerase (Stratagene) from human brain cDNAs using 5′-GTCAGGATCCACCACCATGGAAGCCCCTGAATACC-3′ as the forward primer and 5′-ATATCTCGAGTGCTGCCTTATTCTTTCCTTTG-3′ as the reverse primer and inserted in-frame into the *Bam*HI and *Xho*I sites of the pcDNA3.1/V5His vector (Invitrogen). A plasmid for DsRed-tagged synphilin-1 was constructed by PCR amplification using 5′-ATATCTCGAGACCACCATGGAAGCCCCTGAATACC-3′ as the forward primer and 5′-GTCAGGATCCGCCTTTGCCTTATTCTTTCCTTTG-3′ as the reverse primer and inserted in-frame into the *Xho*I and *Bam*HI sites of the pDsRed-N1 vector (Clontech). A series of deletion mutants of synphilin-1 were prepared as synphilin-1-N (amino acid 1–348), synphilin-1-M (amino acid 349–555), and synphilin-1-C (amino acid 556–919). Synphilin-1-M is the central portion of synphilin-1, containing the ankyrin-like repeat, the coiled-coil domain, and the ATP/GTP-binding domain (31). Primers pairs for each deletion mutant were as follows: 5′-GTCAGGATCCACCACCATGGAAGCCCCTGAATACC-3′ and 5′-ATATCTCGAGTTCGTCGTGAATTTTGTCT-3′ for synphilin-1-N-V5, 5′-ATATCTCGAGACCACCATGGAAGCCCCTGAATACC-3′ and 5′-GTCAGGATCCGCTTCGTCGTGAATTTTGTCTAG-3′ for synphilin-1-N-DsRed, 5′-GTCAGGATCCACCATGAATGGAAACAATCTAT-3′ and 5′-ATATCTCGAGCTTGCCCTCTGATTTCTGG-3′ for synphilin-1-M-V5, 5′-ATATCTCGAGACCACCATGAATGGAAACAATCTAT-3′ and 5′-GTCAGGATCCGCC TTGCCCTCTGATTTCTGGGC-3 for synphilin-1-M-DsRed, 5′-GTCAGGATCCACCACCATGTCACTCCCTTCTTCAC-3′ and 5′-ATATCTCGAGTGCTGCCTTATTCTTTCCTTTG-3′ for synphilin-1-C-V5, and 5′-ATATCTCGAGACCACCATGTCACTCCCTTCTTCAC-3′ and 5′-GTCAGGATCCGCCTTTGCCTTATTCT-

TTCCTTTG-3′ for synphilin-1-C-DsRed. Construction of pcDNA4/HisMax-Dorfin, pcDNA3.1(+)FLAG-ubiquitin, and pcDNA3.1/MycHis(+)-SOD1 vectors was described elsewhere (40, 44). α-Synuclein cDNA was amplified by PCR from human brain cDNAs and cloned into the *Eco*RV site of pcDNA3.1/MycHis(+) (Invitrogen). To generate the mutant α-synuclein expression vector, A30P and A53T mutations were introduced into pcDNA3.1/MycHis(+)-α-synuclein with a QuikChange site-directed mutagenesis kit (Stratagene) following the method of Lee *et al.* (46). COS-7, HEK293, and Neuro2a cells were maintained in Dulbecco's modified Eagle's medium with 10% fetal calf serum. Transfections were performed using the Effectene transfection reagent (QIAGEN Inc.) according to the manufacturer's instructions. To inhibit cellular proteasome activity, cells were treated with 0.5 μM MG132 (carbobenzoxy-L-leucyl-L-leucyl-L-leucinal, Sigma) for 16 h overnight after transfection.

Immunoprecipitation and Western Blot Analysis—Cells were lysed in lysis buffer (50 mM Tris, 150 mM NaCl, 1% Nonidet P-40, and 0.1% SDS) with Complete protease inhibitor mixture (Roche Diagnostics). Immunoprecipitation from transfected cell lysates was performed with 2 μg of antibody and protein A/G Plus-agarose (Santa Cruz Biotechnology), and the immunoprecipitate was then washed four times with lysis buffer. Anti-V5 antibody (Invitrogen) for synphilin-1-V5 fusion proteins and anti-Myc antibody (A-14, Santa Cruz Biotechnology) for α-synuclein-Myc or SOD1-Myc fusion proteins were used. Immunoprecipitates were subjected to SDS-PAGE and analyzed by Western blotting with ECL detection reagents (Amersham Biosciences).

In Vitro Ubiquitylation Assay—Immunopurified (IP) Xpress-Dorfin bound to anti-Xpress antibody (Invitrogen) with protein A/G Plus-agarose (Santa Cruz Biotechnology) was prepared from lysates of HEK293 cells transfected with pcDNA4/HisMax-Dorfin. IP-synphilin-1-V5 was prepared with anti-V5 antibody bound to protein A/G Plus-agarose from lysates of HEK293 cells transfected with pcDNA3.1/V5His-synphilin-1. IP-α-synuclein-Myc and IP-SOD1-Myc were prepared with anti-Myc antibodies from lysates of pcDNA3.1/MycHis(+)-α-synuclein- and pcDNA3.1/MycHis(+)-SOD1-transfected HEK293 cells, respectively. Slurries of IP-Xpress-Dorfin were mixed with IP-synphilin-1-V5, IP-α-synuclein-Myc, or IP-SOD1-Myc and incubated at 30 °C for 90 min in 50 μl of reaction buffer containing ATP (4 mM ATP in 50 mM Tris-HCl (pH 7.5), 2 mM $MgCl_2$, and 2 mM dithiothreitol), 100 ng of rabbit E1 (Calbiochem), 2 μg of UbcH7 (Affiniti), and 2 μg of His-ubiquitin (Calbiochem). The reaction was terminated by adding 20 μl of 4× sample buffer, and 20-μl aliquots of the reaction mixtures were subjected to SDS-PAGE, followed by Western blotting with anti-His antibody (Novagen).

Neurotoxicity Analysis and Quantification of Synphilin-1 Aggregates—COS-7 cells (1×10^4) were grown overnight on collagen-coated 4-chamber well slides. They were transfected with 0.2 μg of pDsRed-N1-synphilin-1 or its deletion mutants. To inhibit cellular proteasome activity, cells were treated with 0.5 μM MG132 for 16 h overnight after transfection. The number of inclusions was counted in >100 cells randomly selected, and data were averaged from three independent experiments. For cell viability assay, 5×10^3 Neuro2a cells were grown in collagen-coated 96-well plates overnight. They were then transfected with 0.1 μg of pcDNA3.1/V5His-synphilin-1 or deletion mutants of synphilin-1. pcDNA3.1/V5His-LacZ was used as a control. Next, an MTS-based cell proliferation assay was performed using CellTiter 96 (Promega) at 24 h after serum deprivation. The assay was carried out in triplicate. Absorbance at 490 nm was measured in a multiple plate reader.

RESULTS

Dorfin Localizes to LBs of PD—We first examined whether LBs contain Dorfin. Immunohistochemical analysis revealed that Dorfin was predominantly localized in LBs found in PD (Fig. 1*A*). The peripheral rim of a typical LB in a neuronal cell body was strongly stained, whereas the central core remained unstained (Fig. 1*B*). Dorfin was also localized in Lewy neurites (Fig. 1*C*), which are a pathological hallmark in addition to LBs of degenerating neurons in the brains of patients suffering from PD (47). Anti-Dorfin antibody did not stain any abnormal structures in normal brains (data not shown). A double-labeling immunofluorescence study revealed that Dorfin was colocalized with ubiquitin in LBs (Fig. 1, *D–F*). Serial sections stained with anti-Dorfin and anti-ubiquitin antibodies showed that ~90% of ubiquitylated LBs were positive for Dorfin immunoreactivity. The staining profile of Dorfin was very similar to that of α-synuclein (48), which is predominantly located in the peripheral rim of LBs, but was different from that of parkin, which localizes predominantly in the core of LBs (49).

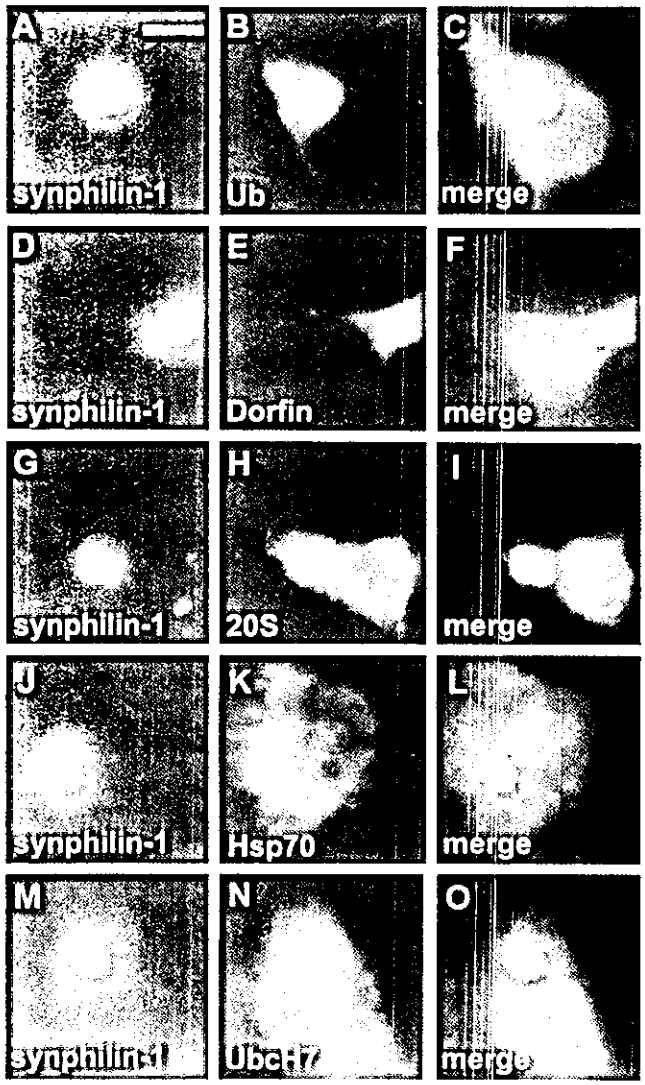

FIG. 2. **Formation of large juxtanuclear inclusions by overexpression of synphilin-1.** Full-length synphilin-1 was overexpressed in COS-7 cells as DsRed fusion protein. Two days after transfection, cells were fixed and immunostained with the indicated antibodies. Large juxtanuclear inclusions of synphilin-1 were formed spontaneously without proteasome inhibition. Cells with large juxtanuclear inclusions were co-stained with ubiquitin (*Ub*) (*A–C*), Dorfin (*D–F*), 20 S proteasome core subunit (*G–I*), Hsp70 (*J–L*), or UbcH7 (*M–O*). Regions of overlap between synphilin-1 (*red*) and immunoreactivities of the indicated proteins (*green*) are shown in *yellow*. Nuclei were stained with Hoechst 33342 (*blue*). *Scale bar* = 10 μm.

Expression of Synphilin-1 Induces LB-like Large Juxtanuclear Inclusions, and Dorfin Localizes to These Inclusions—To investigate the relationships of Dorfin to components of LBs other than ubiquitin, we first examined the subcellular localization of α-synuclein and synphilin-1 in cultured cells. We created wild-type and mutant α-synuclein-green fluorescent protein and α-synuclein-Myc fusion constructs, but there was no evidence of α-synuclein aggregation in transfected COS-7 cells in the presence or absence of the proteasome inhibitor (data not shown). We created a synphilin-1-DsRed fusion construct by fusing the red fluorescent protein DsRed to the C terminus of synphilin-1 and carried out transient transfection in COS-7 cells with this construct. Large juxtanuclear inclusions were spontaneously formed in the transfected COS-7 cells in the absence of the proteasome inhibitor (Fig. 2, *A–O*). We

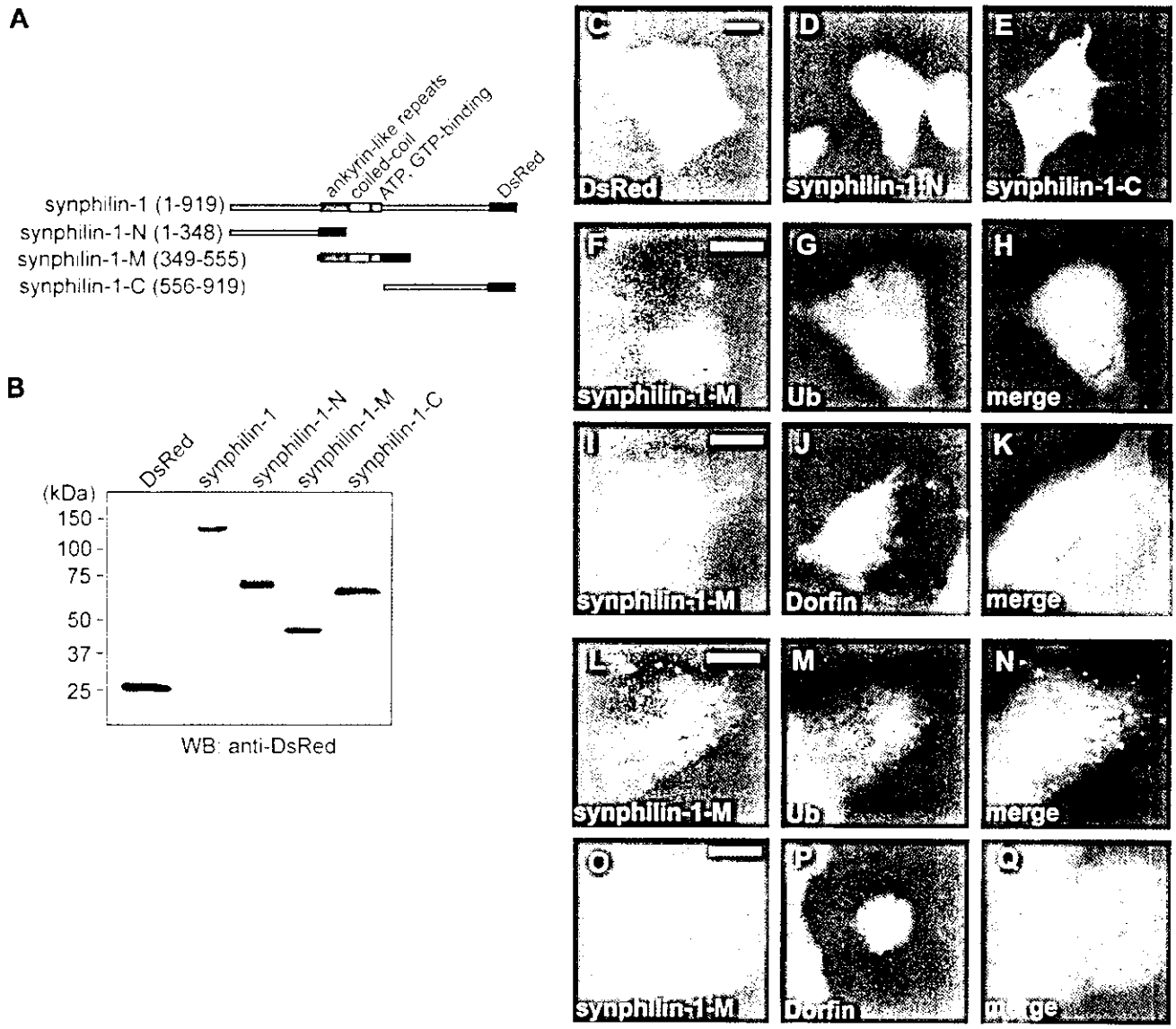

FIG. 3. **Formation of two types of aggregates by the central portion of synphilin-1.** COS-7 cells were transfected with expression vectors for DsRed alone or DsRed fusion proteins of synphilin-1 deletion mutants. Two days after transfection, cells were analyzed by Western blotting (*WB*) and immunocytochemistry. Shown are a schematic representation of the DsRed fusion proteins of synphilin-1 deletion mutants used in this study (*A*) and the results from Western blot analysis of lysates from transfected cells (*B*). DsRed alone (*C*), synphilin-1-N (*D*), and synphilin-1-C (*E*) formed no aggregates, whereas overexpression of the central portion of synphilin-1 (synphilin-1-M) induced two types of inclusions: large juxtanuclear inclusions (*F* and *I*) and small punctate aggregates scattered throughout the cytoplasm (*L* and *O*). Large juxtanuclear inclusions were ubiquitin (*Ub*)-positive (*F–H*) and colocalized with Dorfin (*I–K*), whereas small punctate aggregates were ubiquitin-negative (*L–N*) and did not colocalize with Dorfin (*O–Q*). Regions of overlap between synphilin-1 (*red*) and immunoreactivities of the indicated proteins (*green*) are shown in *yellow*. Nuclei were stained with Hoechst 33342 (*blue*). *Scale bar* = 10 μm.

also constructed synphilin-1 fusion proteins with a smaller V5/His_6 tag, which formed identical inclusions when overexpressed in COS-7 cells, although to a lesser extent than synphilin-1-DsRed fusion proteins (data not shown). Immunostaining with anti-ubiquitin and anti-Dorfin antibodies revealed that most of the large juxtanuclear inclusions of synphilin-1 contained ubiquitin (Fig. 2, *A–C*) and Dorfin (*D–F*). Immunohistochemical studies of human LBs have previously shown that LBs are stained with proteasome subunits (6) and molecular chaperones such as Hsp40 and Hsp70 (24). Thus, we next examined whether the inclusion bodies in COS-7 cells contain the 20 S proteasome core subunit and Hsp70. We found both the 20 S proteasome subunit and Hsp70 to be colocalized with synphilin-1 inclusion bodies (Fig. 2, *G–L*). Dorfin binds specifically to UbcH7 as an E2 through the RING finger/IBR domain (40). UbcH7 was also localized with Dorfin in these inclusions (Fig. 2, *M–O*). These observations suggest that large juxtanuclear inclusions formed by synphilin-1 in our cell culture system have many characteristic features of LBs, that synphilin-1 can aggregate when overexpressed, and that this process may be associated with its ubiquitylation.

Expression of the Central Portion of Synphilin-1 Induces Large Juxtanuclear Inclusions as Full-length Proteins, but Small Punctate Aggregates Are Also Formed—To further analyze which part of synphilin-1 is related to aggregation formation, we prepared a series of deletion mutants of synphilin-1. We divided synphilin-1 into three parts, the N terminus of synphilin-1 (synphilin-1-N) containing amino acids 1–348, the central portion of synphilin-1 (synphilin-1-M) containing amino acids 349–555, and the C terminus of synphilin-1 (synphilin-1-C) containing amino acids 556–919, and fused them to DsRed at their C termini (Fig. 3, *A* and *B*). Inclusions were not seen with overexpression of DsRed alone, synphilin-1-N, or synphilin-1-C in COS-7 cells (Fig. 3, *C–E*). However, expression of

synphilin-1-M resulted in the production of two types of inclusions: large juxtanuclear inclusions (Fig. 3, *F–K*) and small punctate aggregates scattered throughout the cytoplasm (*L–Q*). The large inclusions were stained with ubiquitin (Fig. 3, *F–H*) and Dorfin (*I–K*), as were inclusions induced by full-length synphilin-1. However, neither ubiquitin nor Dorfin was colocalized with the small punctate aggregates scattered throughout the cytoplasm (Fig. 3, *L–Q*).

Expression of the Central Portion of Synphilin-1 Compromises Cell Viability—We examined the frequency of the inclusion formation by synphilin-1 and its deletion mutants. The number of inclusions was counted with and without the proteasome inhibitor MG132 in COS-7 cells (Fig. 4*A*). Both synphilin-1-N and synphilin-1-C formed almost no inclusions in either the presence or absence of MG132. Full-length synphilin-1 and synphilin-1-M produced inclusions with high frequency even in the absence of MG132, and the number of cells with inclusions induced by full-length synphilin-1 was significantly greater than that induced by synphilin-1-M (Fig. 4*A*). Treatment with MG132 significantly increased the number of inclusions. We next measured the ratio of cells that contained small punctate aggregates to total cells bearing all inclusions (Fig. 4*B*) because two types of aggregates, large juxtanuclear inclusions and small punctate scattered aggregates, were observed. In contrast to full-length synphilin-1, the inclusions induced by overexpression of synphilin-1-M were predominantly small punctate aggregates scattered through the cytoplasm (Fig. 4*B*). Treatment with MG132 decreased the ratio of small aggregates induced by synphilin-1-M (Fig. 4*B*).

The effects of synphilin-1 expression on cell viability are poorly understood. O'Farrell *et al.* (36) reported that cells transfected with synphilin-1 are more viable than cells transfected with LacZ. On the other hand, Lee *et al.* (37) reported that synphilin-1 compromises cell viability. Thus, we examined the effects of synphilin-1 and its deletion mutants on cell viability using the MTS assay in the neuronal cell line Neuro2a (Fig. 4*C*). We found that synphilin-1-M had a cytotoxic effect, whereas overexpression of full-length synphilin-1 or the N- or C-terminal deletion mutant of synphilin-1 did not (Fig. 4*C*). We used synphilin-1-V5 fusion constructs, but synphilin-1-DsRed fusion constructs gave the same results (data not shown).

Dorfin Interacts with Synphilin-1—We examined whether Dorfin interacts with synphilin-1 because Dorfin localizes in LBs and cytoplasmic juxtanuclear inclusions formed by synphilin-1. To identify which portion of synphilin-1 binds to Dorfin, we expressed a series of deletion mutants of V5-tagged synphilin-1 and Xpress-tagged Dorfin in COS-7 cells (Fig. 5*B*). Coimmunoprecipitation confirmed that Dorfin bound to full-length synphilin-1 (Fig. 5*A*) and interacted strongly with synphilin-1-M and weakly with synphilin-1-N, but Dorfin failed to bind to synphilin-1-C (Fig. 5*C*). Thus, Dorfin interacts with synphilin-1 mainly through its central portion, which contains the ankyrin-like repeat, the coiled-coil domain, and the ATP/GTP-binding domain. Dorfin has a unique primary structure containing a RING finger/IBR motif at its N terminus and can be structurally divided into two parts, the N-terminal region containing a RING finger/IBR motif (Dorfin-N) that interacts with E2 and the C-terminal region with no similarity to any other known proteins (Dorfin-C) (Fig. 5*B*) (40). We found that Dorfin-C, but not Dorfin-N, specifically bound synphilin-1, indicating that Dorfin binds to synphilin-1 via its C-terminal region (Fig. 5*D*).

Dorfin Ubiquitylates Synphilin-1 through Its Central Domain In Vitro—The physical interaction between Dorfin and synphilin-1 prompted us to investigate whether synphilin-1 itself is ubiquitylated by Dorfin. We first examined whether

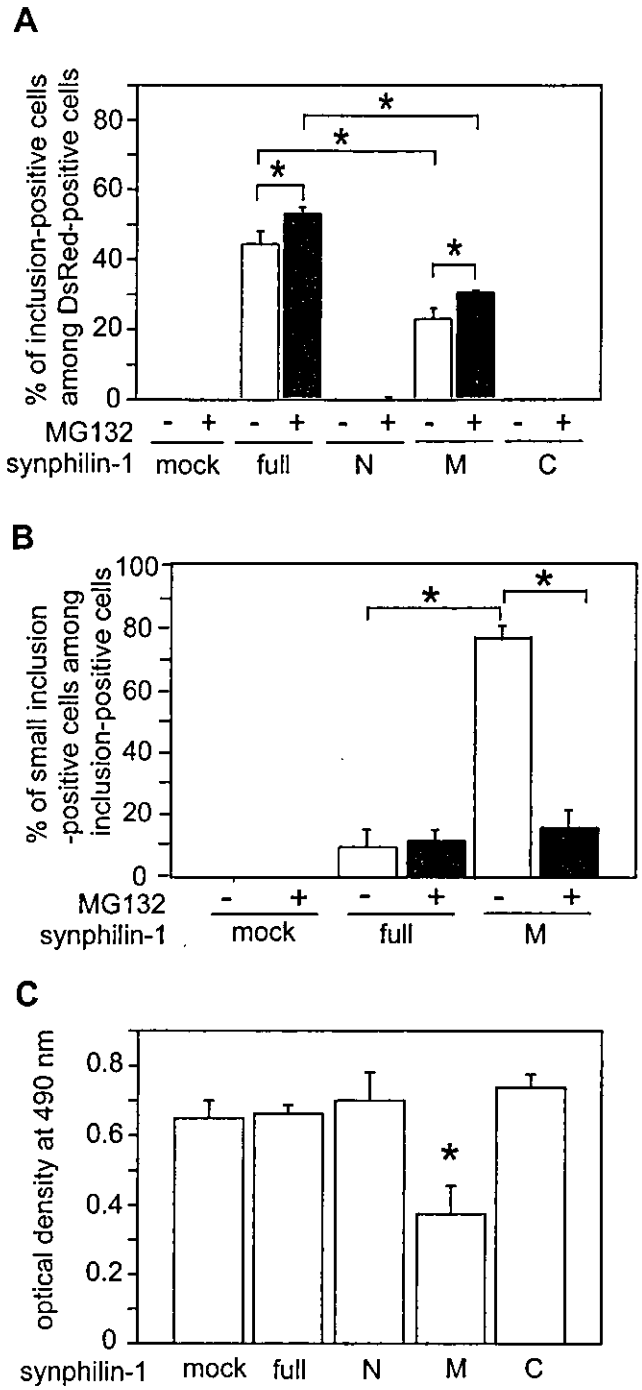

FIG. 4. **The central portion of synphilin-1 produces predominantly small punctate aggregates and compromises cell viability.** *A*, the frequency of inclusion-bearing cells transfected with synphilin-1 and its deletion mutants. COS-7 cells were grown on collagen-coated 4-chamber well slides and transfected with expression vectors for synphilin-1-DsRed fusion proteins. Two days after transfection, cells were fixed, and percentages of inclusion-positive cells among DsRed-positive cells were determined. For proteasome inhibition, cells were treated with 0.5 μM MG132 for 16 h before fixation. *B*, the frequency of cells bearing small punctate aggregates scattered through the cytoplasm among all inclusion-positive cells. Experimental conditions were same as described for *A*. Data are the means ± S.D. of triplicate assays. Statistical analyses were carried out with Mann-Whitney's *U* test. *, $p < 0.01$. *C*, the cytotoxic effect of synphilin-1-M expression in an MTS assay. Neuro2a cells were grown on collagen-coated 96-well plates and transfected with V5-tagged synphilin-1 or its deletion mutants. After changing to a serum-free medium, MTS assays were performed after 24 h of incubation. Viability of cells was measured as the level of absorbance at 490 nm. Data are means ± S.D. of triplicate assays. Statistical analyses were carried out by one-way analysis of variance. *, $p < 0.01$.

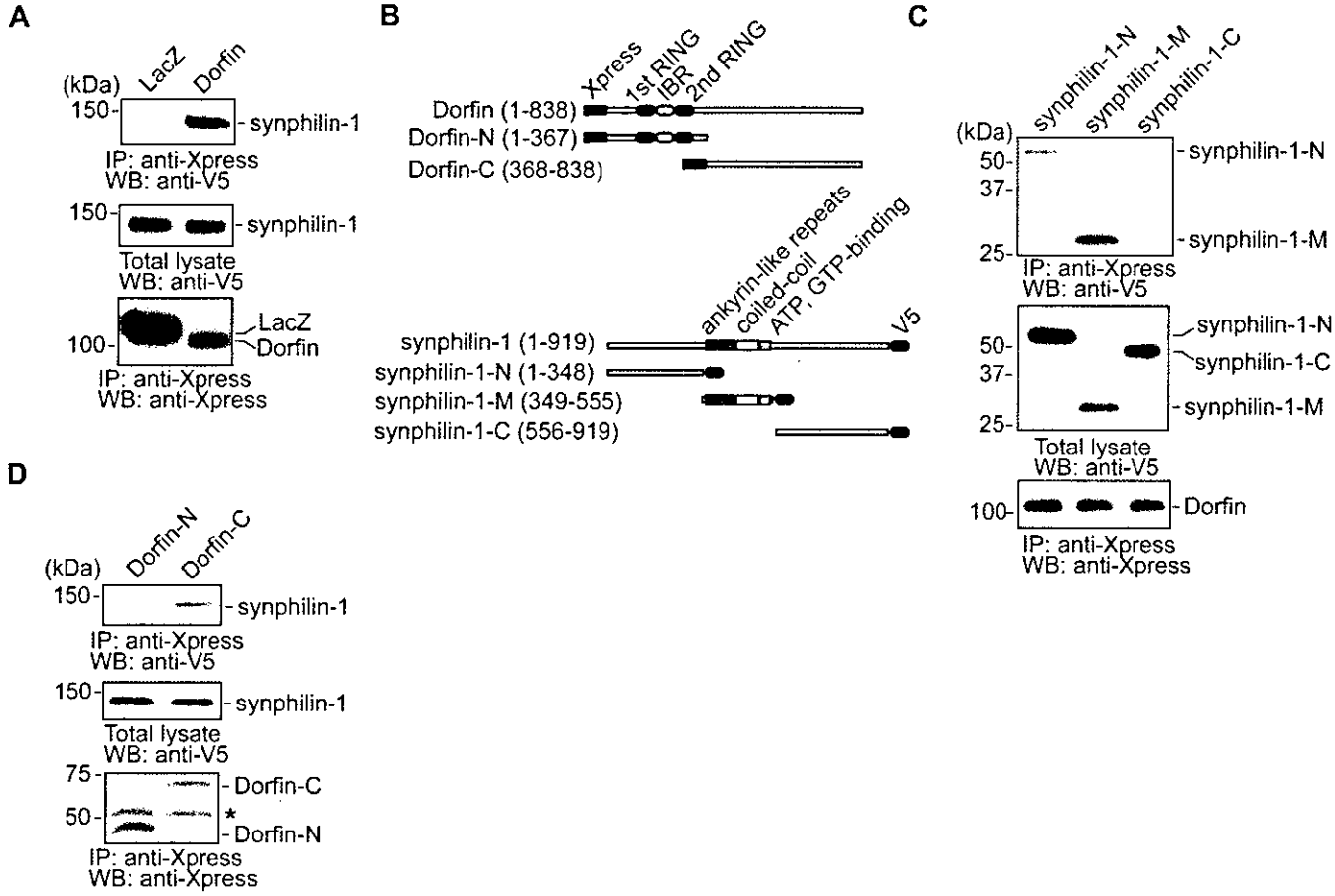

FIG. 5. **Association of Dorfin with synphilin-1 in COS-7 cells.** *A*, Dorfin binds to synphilin-1. V5-tagged synphilin-1 or LacZ was cotransfected with Xpress-tagged Dorfin in COS-7 cells. After immunoprecipitation (*IP*) was performed with anti-Xpress antibody, the resulting precipitates and cell lysate were analyzed by Western blotting (*WB*) with horseradish peroxidase-conjugated anti-V5 or anti-Xpress antibody. *B*, schematic representation of Xpress-tagged Dorfin, deletion mutants of Dorfin (*i.e.* Dorfin-N and Dorfin-C), V5-tagged synphilin-1, and deletion mutants of synphilin-1 (*i.e.* synphilin-1-N, synphilin-1-M, and synphilin-1-C) used in this study. *C*, Dorfin binds to synphilin-1 mainly through its central portion. After V5-tagged deletion mutants of synphilin-1 and Xpress-tagged Dorfin were transfected, immunoprecipitation and Western blotting were performed as described for *A*. *D*, binding of synphilin-1 to the C-terminal portion of Dorfin. After V5-tagged synphilin-1 and Xpress-tagged deletion mutants of Dorfin were transfected, immunoprecipitation and Western blotting were performed as described for *A*.

synphilin-1 is ubiquitylated in a culture cell model. V5-tagged full-length synphilin-1 or its deletion mutants were cotransfected with FLAG-tagged ubiquitin in HEK293 cells. When full-length synphilin-1 or its deletion mutants were immunoprecipitated after treatment with the proteasome inhibitor MG132, full-length synphilin-1 and synphilin-1-M were found to be polyubiquitylated, but synphilin-1-N and synphilin-1-C were not (Fig. 6*A*). Wild-type and mutant α-synuclein were found not to be polyubiquitylated, whereas, as previously reported (44), mutant SOD1 was polyubiquitylated (Fig. 6*A*).

We next examined whether Dorfin is involved in the ubiquitylation of synphilin-1 *in vitro*. For this purpose, we immunopurified Xpress-Dorfin and synphilin-1-V5 independently after transfection into HEK293 cells. When these immunopurified proteins were incubated with recombinant E1, E2 (UbcH7), His-tagged ubiquitin, and ATP, high molecular mass ubiquitylated bands were observed in the presence of Xpress-Dorfin with synphilin-1, whereas no signal was noted with synphilin-1 in the absence of either E1 or E2 (Fig. 6*B*). Dorfin ubiquitylated mutant SOD1 *in vitro*, as previously reported (44). Dorfin did not ubiquitylate either wild-type or mutant α-synuclein (Fig. 6*B*). *In vitro* ubiquitylation assay of a series of synphilin-1 deletion mutants with Dorfin revealed that synphilin-1-M was ubiquitylated, whereas synphilin-1-N and synphilin-1-C were not ubiquitylated at all (Fig. 6*C*).

DISCUSSION

Several lines of evidence have suggested that derangements in the ubiquitin-proteasome protein degradation pathway may have a prominent role in the pathogenesis of PD (5). Our present study shows that Dorfin, an E3 ubiquityl ligase, is colocalized with ubiquitin in LBs of PD and physically binds to ubiquitylate synphilin-1, which is known to be a major component of LBs (31, 38, 39).

For the analysis of LB formation by synphilin-1, various cell culture models have been reported (31, 35–37). In our cell culture model, overexpression of synphilin-1 alone induced large juxtanuclear cytoplasmic inclusions. In these large inclusions, Dorfin was colocalized with ubiquitin/proteasome pathway-related proteins such as ubiquitin, the 20 S proteasome core subunit, and Hsp70, just as Dorfin in LBs. The central portion of synphilin-1 contains the ankyrin-like repeat, the coiled-coil domain, and the ATP/GTP-binding domain (31). This region is reported to be necessary for interaction with α-synuclein (32). We found that the central portion of synphilin-1 also bound with Dorfin and that overexpression of this region alone led to inclusion body formation, whereas neither the N- nor C-terminal regions induced aggregates. Overexpression of this central portion of synphilin-1 produced small punctate aggregates scattered throughout the cytoplasm as well as large juxtanuclear inclusions, but the former predominated.

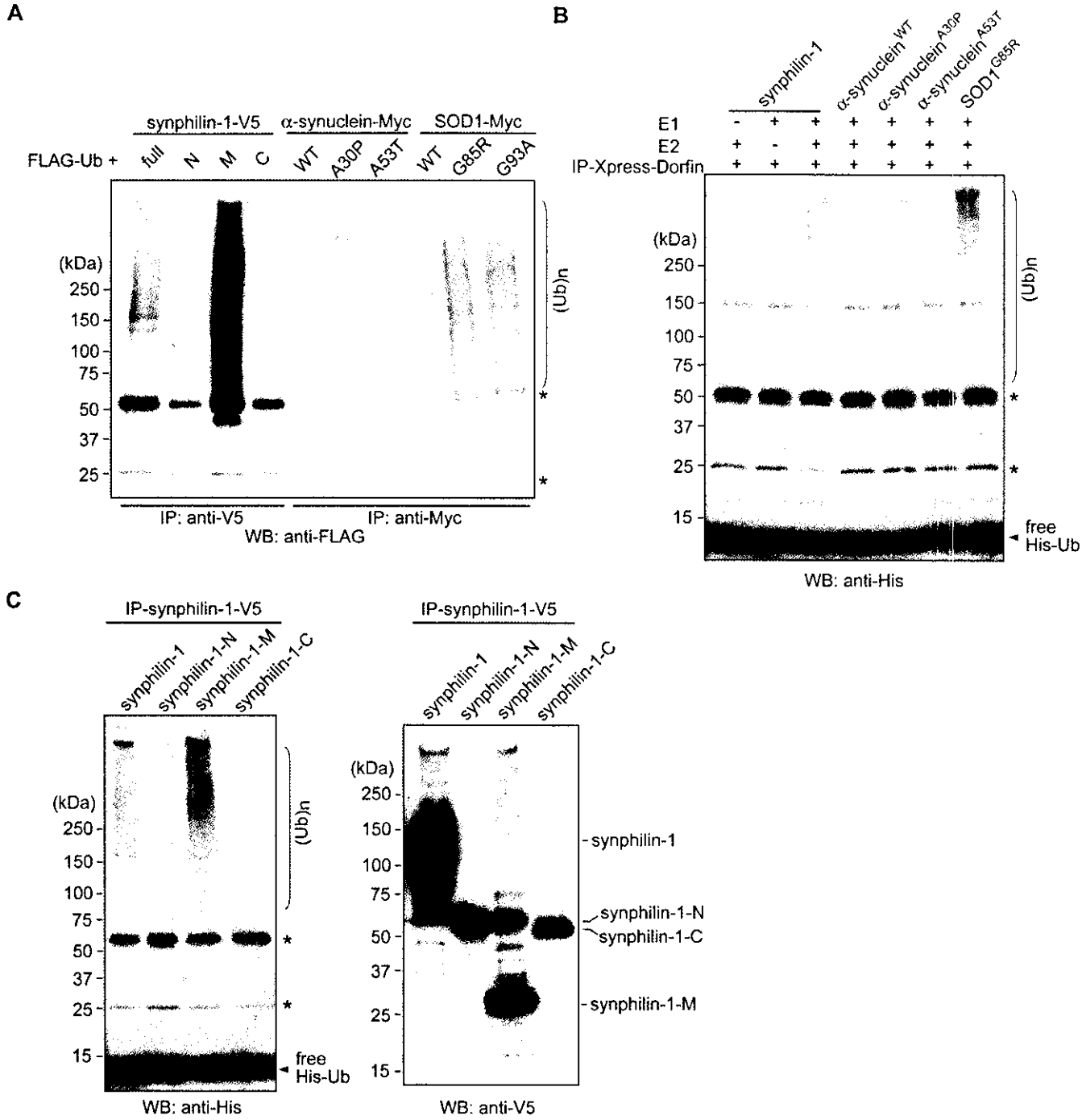

FIG. 6. **Ubiquitylation of synphilin-1 by Dorfin.** *A*, synphilin-1 is ubiquitylated in HEK293 cells. V5-tagged synphilin-1 or its deletion mutants were cotransfected with FLAG-tagged ubiquitin (*Ub*) in HEK293 cells and treated with 0.5 μM MG132 for 16 h overnight after transfection. Myc-tagged α-synuclein or SOD1 was cotransfected with FLAG-ubiquitin and treated as described above. Immunoprecipitates (*IP*) prepared with anti-V5 or anti-Myc antibody were used for immunoblotting with anti-FLAG antibody. *B*, *in vitro* ubiquitylation assay of synphilin-1 with Dorfin. Xpress-tagged Dorfin and V5-tagged synphilin-1 were transfected into HEK293 cells independently. Immunopurified Dorfin (IP-Xpress-Dorfin) and synphilin-1 (IP-synphilin-1-V5) were prepared and mixed in an assay mixture for ubiquitylation. For this assay, Myc-tagged wild-type (*WT*) and mutant α-synuclein and Myc-tagged mutant SOD1(G85R) were also used instead of synphilin-1. After a 90-min incubation at 30 °C, SDS-PAGE was performed, followed by Western blotting (*WB*) for His-tagged ubiquitin with anti-His antibody. *C*, *in vitro* ubiquitylation assay of various synphilin-1 deletion mutants with Dorfin. V5-tagged deletion mutants of synphilin-1 were transfected into HEK293 cells, immunopurified, and mixed with IP-Xpress-Dorfin in an assay mixture for ubiquitylation as described for *B*. The reaction products were analyzed by Western blotting with anti-His antibody for ubiquitin (*left panel*) and with anti-V5 antibody for synphilin-1 (*right panel*). High molecular mass ubiquitylated synphilin-1 and synphilin-1-M are shown as (*Ub*)*n*. *Asterisks* indicate IgG light and heavy chains.

The small punctate aggregates did not colocalize with either ubiquitin or other proteasome pathway-associated proteins and had cytotoxic effects as revealed by MTS assays. Recently, Lee and Lee (50) reported that overexpression of α-synuclein in culture cells produces two distinct types of aggregates: large juxtanuclear inclusions and small punctate aggregates scattered throughout the cytoplasm. The juxtanuclear inclusion bodies are filled with amyloid-like α-synuclein fibrils, whereas the small aggregates contain non-fibrillar spherical aggregates (50). They suggested that these aggregates appear sequentially, with the smallest population appearing first and the fibrillar inclusions last, and that the small spherical aggre-

gates are the cellular equivalents of protofibrils (50). Protofibrils are recognized to be more important in terms of cytotoxicity than mature fibrils in Aβ (51, 52) and α-synuclein (53, 54). In our cell culture model, overexpression of synphilin-1 produced two distinct types of aggregates, very closely resembling two types of α-synuclein aggregates (50). Thus, the small punctate aggregates scattered throughout the cytoplasm induced by the central portion of synphilin-1 might have characteristics similar to those of protofibrils. Our cell culture system will allow detailed characterization of LB formation and cytotoxic processes in further studies.

We reported previously that Dorfin localizes in the inclusion bodies of familial ALS with SOD1 mutations as well as in those of sporadic ALS and ubiquitylates various SOD1 mutants derived from familial ALS patients (44). Based on these findings, it is conceivable that familial and sporadic forms of ALS share a common mechanism involving the dysfunction of the ubiquitin/proteasome pathway, despite having distinct etiological mechanisms. In sporadic ALS, unknown substrate(s) of Dorfin might play a role in the pathogenesis of the disease and accumulate in ubiquitylated inclusion bodies. The following results support the view that Dorfin plays an important role in the formation of LBs of PD: (i) the presence of Dorfin in LBs and large juxtanuclear inclusions of synphilin-1 in our cell culture model, (ii) the parallel distribution patterns of ubiquitin and Dorfin in LBs and inclusion bodies induced by synphilin-1 in cultured cells, and (iii) the E3 function of Dorfin to ubiquitylate synphilin-1. Dorfin did not ubiquitylate either wild-type or mutant α-synuclein; however, our results cannot exclude the possibility that post-translational modification, such as glycosylation (55) or phosphorylation (56, 57), of α-synuclein may be necessary for it to become a substrate for Dorfin because overexpressed α-synuclein was not phosphorylated in our cell culture system (data not shown). The relation between Dorfin and PD shows striking similarities to the relation between Dorfin and ALS. Our findings raise the possibility that PD and ALS are etiologically distinct, but share a biochemically common metabolic pathway through Dorfin, leading to the formation of ubiquitylated inclusion bodies and to neuronal cell degeneration.

Parkin has been shown to have E3 ubiquityl ligase activity (10–12). It was recently demonstrated that an *O*-glycosylated α-synuclein (55) and synphilin-1 (35) are the substrates of parkin and that parkin localizes to LBs of sporadic PD (49). The link between sporadic and familial forms of PD through α-synuclein, synphilin-1, and parkin sheds new light on underlying common molecular pathogenic mechanisms in PD. What roles, then, do Dorfin and parkin play with respect to each other in the pathogenesis of PD and/or LB formation? Both proteins have a RING finger/IBR domain and E3 ubiquitin ligase activities. Parkin interacts with both α-synuclein (55) and synphilin-1 (35), whereas Dorfin binds and ubiquitylates only synphilin-1. Parkin resides in the core of LBs (49), whereas Dorfin localizes predominantly to the rim. Impaired function of parkin as an E3 ubiquityl ligase is responsible for one of the most common forms of familial PD, autosomal recessive juvenile parkinsonism (9, 10). However, there has been no analysis of whether *Dorfin* gene mutation causes familial PD. Recently, Valente *et al.* (58, 59) identified a locus, *PARK6*, on chromosome 1p35–1p36 that is involved in the autosomal recessive form of parkinsonism. Interestingly, a human paralog of Dorfin (Dj1174N9.1) has been mapped at 1p34.1–1p35.3 (60). Furthermore, Dorfin was identified by a phage display system to be one of the binding proteins with 2-methylnorharman, an analog of the parkinsonism-inducing toxin, 1-methyl-4-phenylpyridinium cation (61). These findings suggest the utility of analyzing Dj1174N9.1 or Dorfin mutation for potential involvement in familial PD. Production of Dorfin knockout mice will also answer the question of whether Dorfin is essential for pathogenesis and/or ubiquitylated inclusion body formation in PD.

Acknowledgment—We thank Dr. Miya Kobayashi (Kinjo Gakuin University) for helpful comments.

REFERENCES

1. Forno, L. S. (*J. Neuropathol. Exp. Neurol.* **55,** 259–27, 1996
2. Gibb, W. R., and Lees, A. J. (1988) *J. Neurol. Neurosurg. Psychiatry* **51,** 745–752
3. Olanow, C. W., and Tatton, W. G. (1999) *Annu. Rev. Neurosci.* **22,** 123–144
4. McKeith, I. G. (2000) *Ann. N. Y. Acad. Sci.* **920,** 1–8
5. McNaught, K. S., Olanow, C. W., Halliwell, B., Isacson, O., and Jenner, P. (2001) *Nat. Rev. Neurosci.* **2,** 589–594
6. Iwatsubo, T., Yamaguchi, H., Fujimuro, M., Yokosawa, H., Ihara, Y., Trojanowski, J. Q., and Lee, V. M. (1996) *Am. J. Pathol.* **148,** 1517–1529
7. Ii, K., Ito, K., Tanaka, K., and Hirano, A. (1997) *J. Neuropathol. Exp. Neurol.* **56,** 125–131
8. McNaught, K. S., and Jenner, P. (2001) *Neurosci. Lett.* **297,** 191–194
9. Furukawa, Y., Vigouroux, S., Wong, H., Guttman, M., Rajput, A. H., Ang, L., Briand, M., Kish, S. J., and Briand, Y. (2002) *Ann. Neurol.* **51,** 779–782
10. Kitada, T., Asakawa, S., Hattori, N., Matsumine, H., Yamamura, Y., Minoshima, S., Yokochi, M., Mizuno, Y., and Shimizu, N. (1998) *Nature* **392,** 605–608
11. Shimura, H., Hattori, N., Kubo, S., Mizuno, Y., Asakawa, S., Minoshima, S., Shimizu, N., Iwai, K., Chiba, T., Tanaka, K., and Suzuki, T. (2000) *Nat. Genet.* **25,** 302–305
12. Imai, Y., Soda, M., and Takahashi, R. (2000) *J. Biol. Chem.* **275,** 35661–35664
13. Zhang, Y., Gao, J., Chung, K. K., Huang, H., Dawson, V. L., and Dawson, T. M. (2000) *Proc. Natl. Acad. Sci. U. S. A.* **97,** 13354–13359
14. Leroy, E., Boyer, R., Auburger, G., Leube, B., Ulm, G., Mezey, E., Harta, G., Brownstein, M. J., Jonnalagada, S., Chernova, T., Dehejia, A., Lavedan, C., Gasser, T., Steinbach, P. J., Wilkinson, K. D., and Polymeropoulos, M. H. (1998) *Nature* **395,** 451–452
15. Larsen, C. N., Krantz, B. A., Wilkinson, K. D. (1998) *Biochemistry* **37,** 3358–3368
16. Liu, Y., Fallon, L., Lashuel, H. A., Liu, Z., and Lansbury, P. T., Jr. (2002) *Cell* **111,** 209–218
17. Spillantini, M. G., Schmidt, M. L., Lee, V. M., Trojanowski, J. Q., Jakes, R., and Goedert, M. (1997) *Nature* **388,** 839–840
18. Mezey, E., Dehejia, A., Harta, G., Papp, M. I., Polymeropoulos, M. H., and Brownstein, M. J. (1998) *Nat. Med.* **4,** 755–757
19. Polymeropoulos, M. H., Lavedan, C., Leroy, E., Ide, S. E., Dehejia, A., Dutra, A., Pike, B., Root, H., Rubenstein, J., Boyer, R., Stenroos, E. S., Chandrasekharappa, S., Athanassiadou, A., Papapetropoulos, T., Johnson, W. G., Lazzarini, A. M., Duvoisin, R. C., Di Iorio, G., Golbe, L. I., and Nussbaum, R. L. (1997) *Science* **276,** 2045–2047
20. Kruger, R., Kuhn, W., Muller, T., Woitalla, D., Graeber, M., Kosel, S., Przuntek, H., Epplen, J. T., Schols, L., and Riess, O. (1998) *Nat. Genet.* **18,** 106–108
21. Baba, M., Nakajo, S., Tu, P. H., Tomita, T., Nakaya, K., Lee, V. M., Trojanowski, J. Q., and Iwatsubo, T. (1998) *Am. J. Pathol.* **152,** 879–884
22. Spillantini, M. G., Crowther, R. A., Jakes, R., Hasegawa, M., and Goedert, M. (1998) *Proc. Natl. Acad. Sci. U. S. A.* **95,** 6469–6473
23. Feany, M. B., and Bender, W. W. (2000) *Nature* **404,** 394–398
24. Auluck, P. K., Chan, H. Y., Trojanowski, J. Q., Lee, V. M., and Bonini, N. M. (2002) *Science* **295,** 865–868
25. Masliah, E., Rockenstein, E., Veinbergs, I., Mallory, M., Hashimoto, M., Takeda, A., Sagara, Y., Sisk, A., and Mucke, L. (2000) *Science* **287,** 1265–1269
26. van der Putten, H., Wiederhold, K. H., Probst, A., Barbieri, S., Mistl, C., Danner, S., Kauffmann, S., Hofele, K., Spooren, W. P., Ruegg, M. A., Lin, S., Caroni, P., Sommer, B., Tolnay, M., and Bilbe, G. (2000) *J. Neurosci.* **20,** 6021–6029
27. Kahle, P. J., Neumann, M., Ozmen, L., Muller, V., Jacobsen, H., Schindzielorz, A., Okochi, M., Leimer, U., van der Putten, H., Probst, A., Kremmer, E., Kretzschmar, H. A., and Haass, C. (2000) *J. Neurosci.* **20,** 6365–6373
28. Kahle, P. J., Neumann, M., Ozmen, L., Muller, V., Odoy, S., Okamoto, N., Jacobsen, H., Iwatsubo, T., Trojanowski, J. Q., Takahashi, H., Wakabayashi, K., Bogdanovic, N., Riederer, P., Kretzschmar, H. A., and Haass, C. (2001) *Am. J. Pathol.* **159,** 2215–2225
29. Giasson, B. I., Duda, J. E., Quinn, S. M., Zhang, B., Trojanowski, J. Q., and Lee, V. M. (2002) *Neuron* **34,** 521–533
30. Lee, M. K., Stirling, W., Xu, Y., Xu, X., Qui, D., Mandir, A. S., Dawson, T. M., Copeland, N. G., Jenkins, N. A., and Price, D. L. (2002) *Proc. Natl. Acad. Sci. U. S. A.* **99,** 8968–8973
31. Engelender, S., Kaminsky, Z., Guo, X., Sharp, A. H., Amaravi, R. K., Kleiderlein, J. J., Margolis, R. L., Troncoso, J. C., Lanahan, A. A., Worley, P. F., Dawson, V. L., Dawson, T. M., and Ross, C. A. (1999) *Nat. Genet.* **22,** 110–114
32. Neystat, M., Rzhetskaya, M., Kholodilov, N., and Burke, R. E. (2002) *Neurosci. Lett.* **325,** 119–123
33. Kawamata, H., McLean, P. J., Sharma, N., and Hyman, B. T. (2001) *J. Neurochem.* **77,** 929–934
34. Ribeiro, C. S., Carneiro, K., Ross, C. A., Menezes, J. R., and Engelender, S. (2002) *J. Biol. Chem.* **277,** 23927–23933
35. Chung, K. K., Zhang, Y., Lim, K. L., Tanaka, Y., Huang, H., Gao, J., Ross, C. A., Dawson, V. L., and Dawson, T. M. (2001) *Nat. Med.* **7,** 1144–1150
36. O'Farrell, C., Murphy, D. D., Petrucelli, L., Singleton, A. B., Hussey, J., Farrer,

M., Hardy, J., Dickson, D. W., and Cookson, M. R. (2001) *Brain Res. Mol. Brain Res.* **97,** 94–102
37. Lee, G., Junn, E., Tanaka, M., Kim, Y. M., and Mouradian, M. M. (2002) *J. Neurochem.* **83,** 346–352
38. Wakabayashi, K., Engelender, S., Tanaka, Y., Yoshimoto, M., Mori, F., Tsuji, S., Ross, C. A., and Takahashi, H. (2002) *Acta Neuropathol.* **103,** 209–214
39. Wakabayashi, K., Engelender, S., Yoshimoto, M., Tsuji, S., Ross, C. A., and Takahashi, H. (2000) *Ann. Neurol.* **47,** 521–523
40. Niwa, J.-i., Ishigaki, S., Doyu, M., Suzuki, T., Tanaka, K., and Sobue, G. (2001) *Biochem. Biophys. Res. Commun.* **281,** 706–713
41. Morett, E., and Bork, P. (1999) *Trends Biochem. Sci.* **24,** 229–231
42. Moynihan, T. P., Ardley, H. C., Nuber, U., Rose, S. A., Jones, P. F., Markham, A. F., Scheffner, M., and Robinson, P. A. (1999) *J. Biol. Chem.* **274,** 30963–30968
43. Ardley, H. C., Tan, N. G., Rose, S. A., Markham, A. F., and Robinson, P. A. (2001) *J. Biol. Chem.* **276,** 19640–19647
44. Niwa, J.-i., Ishigaki, S., Hishikawa, N., Yamamoto, M., Doyu, M., Murata, S., Tanaka, K., Taniguchi, N., and Sobue, G. (2002) *J. Biol. Chem.* **277,** 36793–36798
45. Hishikawa, N., Hashizume, Y., Yoshida, M., and Sobue, G. (2001) *Neuropathol. Appl. Neurobiol.* **27,** 362–372
46. Lee, M., Hyun, D., Halliwell, B., and Jenner, P. (2001) *J. Neurochem.* **76,** 998–1009
47. Braak, H., Sandmann-Keil, D., Gai, W., and Braak, E. (1999) *Neurosci. Lett.* **265,** 67–69
48. Takahashi, H., and Wakabayashi, K. (2001) *Neuropathology* **21,** 315–322
49. Schlossmacher, M. G., Frosch, M. P., Gai, W. P., Medina, M., Sharma, N., Forno, L., Ochiishi, T., Shimura, H., Sharon, R., Hattori, N., Langston, J. W., Mizuno, Y., Hyman, B. T., Selkoe, D. J., and Kosik, K. S. (2002) *Am. J. Pathol.* **160,** 1655–1667
50. Lee, H. J., and Lee, S. J. (2002) *J. Biol. Chem.* **277,** 48976–48983
51. Klein, W. L., Krafft, G. A., and Finch, C. E. (2001) *Trends Neurosci.* **24,** 219–224
52. Bucciantini, M., Giannoni, E., Chiti, F., Baroni, F., Formigli, L., Zurdo, J., Taddei, N., Ramponi, G., Dobson, C. M., and Stefani, M. (2002) *Nature* **416,** 507–511
53. Conway, K. A., Lee, S. J., Rochet, J. C., Ding, T. T., Williamson, R. E., and Lansbury, P. T., Jr. (2000) *Proc. Natl. Acad. Sci. U. S. A.* **97,** 571–576
54. Goldberg, M. S., and Lansbury, P. T., Jr. (2000) *Nat. Cell Biol.* **2,** 115–119
55. Shimura, H., Schlossmacher, M. G., Hattori, N., Frosch, M. P., Trockenbacher, A., Schneider, R., Mizuno, Y., Kosik, K. S., and Selkoe, D. J. (2001) *Science* **293,** 263–269
56. Okochi, M., Walter, J., Koyama, A., Nakajo, S., Baba, M., Iwatsubo, T., Meijer, L., Kahle, P. J., and Haass, C. (2000) *J. Biol. Chem.* **275,** 390–397
57. Fujiwara, H., Hasegawa, M., Dohmae, N., Kawashima, A., Masliah, E., Goldberg, M. S., Shen, J., Takio, K., and Iwatsubo, T. (2002) *Nat. Cell Biol.* **4,** 160–164
58. Valente, E. M., Bentivoglio, A. R., Dixon, P. H., Ferraris, A., Ialongo, T., Frontali, M., Albanese, A., and Wood, N. W. (2001) *Am. J. Hum. Genet.* **68,** 895–900
59. Valente, E. M., Brancati, F., Ferraris, A., Graham, E. A., Davis, M. B., Breteler, M. M., Gasser, T., Bonifati, V., Bentivoglio, A. R., De Michele, G., Durr, A., Cortelli, P., Wassilowsky, D., Harhangi, B. S., Rawal, N., Caputo, V., Filla, A., Meco, G., Oostra, B. A., Brice, A., Albanese, A., Dallapiccola, B., and Wood, N. W. (2002) *Ann. Neurol.* **51,** 14–18
60. Marin, I., and Ferrus, A. (2002) *Mol. Biol. Evol.* **19,** 2039–2050
61. Gearhart, D. A., Toole, P. F., and Beach, J. W. (2002) *Neurosci. Res.* **44,** 255–265

Acta Neuropathol (2003) 106 : 112–120
DOI 10.1007/s00401-003-0708-z

REGULAR PAPER

Shinsuke Kato · Hiroshi Funakoshi · Toshikazu Nakamura · Masako Kato · Imaharu Nakano · Asao Hirano
Eisaku Ohama

Expression of hepatocyte growth factor and c-Met in the anterior horn cells of the spinal cord in the patients with amyotrophic lateral sclerosis (ALS): immunohistochemical studies on sporadic ALS and familial ALS with superoxide dismutase 1 gene mutation

Received: 15 October 2002 / Revised: 17 March 2003 / Accepted: 18 March 2003 / Published online: 18 April 2003

Abstract To clarify the trophic mechanism of residual anterior horn cells affected by sporadic amyotrophic lateral sclerosis (SALS) and familial ALS (FALS) with superoxide dismutase 1 (SOD1) mutations, we investigated the immunohistochemical expression of hepatocyte growth factor (HGF), a novel neurotrophic factor, and its receptor, c-Met. In normal subjects, immunoreactivity to both anti-HGF and anti-c-Met antibodies was observed in almost all anterior horn cells, whereas no significant immunoreactivity was observed in astrocytes and oligodendrocytes. Histologically, the number of spinal anterior horn cells in ALS patients decreased along with disease progression. Immunohistochemically, the number of neurons negative for HGF and c-Met increased with ALS disease progression. However, throughout the course of the disease, certain residual anterior horn cells co-expressed both HGF and c-Met with the same, or even stronger intensity in comparison with those of normal subjects, irrespective of the reduction in the number of immunopositive cells. Western blot analysis revealed that c-Met was induced in the spinal cord of a patient with SALS after a clinical course of 2.5 years, whereas the level decreased in a SALS patient after a clinical course of 11 years 5 months. These results suggest that the autocrine and/or paracrine trophic support of the HGF-c-Met system contributes to the attenuation of the degeneration of residual anterior horn cells in ALS, while disruption of the neuronal HGF-c-Met system at an advanced disease stage accelerates cellular degeneration and/or the process of cell death. In SOD1-mutated FALS patients, Lewy body-like hyaline inclusions (LBHIs) in some residual anterior horn cells exhibited co-aggregation of both HGF and c-Met, although the cytoplasmic staining intensity for HGF and c-Met in the LBHI-bearing neurons was either weak or negative. Such sequestration of HGF and c-Met in LBHIs may suggest partial disruption of the HGF-c-Met system, thereby contributing to the acceleration of neuronal degeneration in FALS patients.

Keywords Amyotrophic lateral sclerosis · Hepatocyte growth factor · c-Met · Neurotrophic factor · Lewy body-like hyaline inclusion

S. Kato (✉) · E. Ohama
Department of Neuropathology, Institute of Neurological Sciences, Faculty of Medicine, Tottori University, Nishi-cho 36-1, 683-8504 Yonago, Japan
Tel.: +81-859-348034, Fax: +81-859-348289, e-mail: kato@grape.med.tottori-u.ac.jp

H. Funakoshi · T. Nakamura
Division of Molecular Regenerative Medicine, Course of Advanced Medicine, Osaka University Graduate School of Medicine, 565-0871 Osaka, Japan

M. Kato
Division of Pathology, Tottori University Hospital, Yonago, Japan

I. Nakano
Department of Neurology, Jichi Medical College, Tochigi, Japan

A. Hirano
Division of Neuropathology, Department of Pathology, Montefiore Medical Center, Bronx, New York, USA

Introduction

Amyotrophic lateral sclerosis (ALS), which was first described by Charcot and Joffroy in 1869 [3], is a fatal and age-associated neurodegenerative disorder that primarily involves both the upper and lower motor neurons [11]. This disease has been recognized as a distinct clinicopathological entity of unknown etiology for over 130 years.

Hepatocyte growth factor (HGF) was first identified as a potent mitogen for mature hepatocytes [24] and was cloned in 1989 by Nakamura et al. [25]. Although HGF was discovered as a hepatotrophic factor, recent expression and functional analyses have revealed that HGF is also a neurotrophic factor [8, 21, 23]. HGF exerts neurotrophic effects on the hippocampal, cerebral cortical, midbrain dopaminergic, cerebellar granular, sensory, and motor neurons, as well as on the sympathetic neuroblasts [8, 12, 23]. HGF is one of the most potent *in vitro* survival-promoting